Journal of Environmental Chemical Engineering 14 (2026) 121589

Contents lists available at ScienceDirect

Journal of Environmental Chemical Engineering

journal homepage: www.elsevier.com/locate/jece

Intensified disinfection of aquaculture matrices by Ga_2O_3/UV-C photocatalysis coupled with peracetic acid

Pablo Santiago-Espiñeira, Jorge Rodríguez-Chueca, Patricia García-Muñoz *

Department of Industrial Chemical & Environmental Engineering, Escuela Técnica Superior de Ingenieros Industriales, Universidad Politécnica de Madrid, C/José Gutiérrez Abascal 2, Madrid 28006, Spain

ARTICLE INFO

Keywords:
Advanced oxidation processes
Disinfection
Ga_2O_3
PAA
Photocatalysis
Recirculating aquaculture systems

ABSTRACT

This study explores the effectiveness of Ga_2O_3/UV-C photocatalysis for disinfecting recirculating aquaculture system (RAS) effluents, focusing on the inactivation of *Enterococcus faecalis*. After material characterization, the research optimized key parameters, including UV-C irradiation intensity, Ga_2O_3 dosage, and oxidant selection (peracetic acid and peroxymonosulfate). The Ga_2O_3/UV-C/peracetic acid (PAA) system was identified as the most effective configuration, significantly enhancing disinfection kinetics and halving treatment time compared to the Ga_2O_3/UV-C system alone. In contrast, the addition of potassium peroxymonosulfate (PMS) exhibited an antagonistic effect, indicating non-productive radical consumption pathways. Mechanistic considerations through scavenging experiments revealed that singlet oxygen ($^1O_2$) played a dominant role in the bacterial disinfection for the Ga_2O_3/UV-C system, while hydroxyl radicals ($HO^\bullet$) were the primary oxidative agents in the PAA-intensified process. The study confirmed the recyclability of Ga_2O_3 over multiple treatment cycles, showing sustained disinfection performance without significant loss of activity. Long-term assessments demonstrated fewer regrowth suppression in the Ga_2O_3/UV-C/PAA system, likely due to residual oxidants like peracetic acid and its by-products, which retain antibacterial properties post-treatment. Furthermore, validation in real aquaculture effluents confirmed the robust performance of the optimized systems, showcasing faster inactivation yields in fish tank water compared to simulated aquaculture water, attributed to differences in organic load. Toxicity considerations, featuring DBPs, water quality parameters measurement and phytotoxicity assessment, indicated promising results. This research positions Ga_2O_3/UV-C photocatalysis, particularly when paired with PAA, as a technically viable and sustainable alternative to conventional chemical disinfectants for RAS applications.

1. Introduction

Aquaculture is increasingly recognized as a vital strategy for addressing global food security challenges [1,2]. This role is particularly critical as the expanding human population drives a corresponding rise in food demand, making the development of innovative production methods essential [3]. However, conventional open-net aquaculture faces growing scrutiny. These traditional systems are resource-intensive, operating within the constraints of limited land and water, and are criticized for their negative environmental footprint, which includes the spread of disease, high water consumption, and nutrient pollution (eutrophication) [4,5]. In contrast, Recirculating Aquaculture Systems (RAS) provide a promising solution, facilitating intensive fish and algae cultivation within a closed-loop system [6–8].

However, operating RAS effectively remains challenging [9]. Although these systems allow for controlled cultivation, they are prone to the buildup of organic matter from excretion and feed [10]. This accumulation fosters ideal conditions for the growth of pathogenic bacteria [11]. Two primary management strategies for this problem present significant drawbacks. First, the frequent use of antibiotics, which carries the risk of improper dosing [12], leads to concerns about residual compounds. The incomplete degradation of these antibiotics or their metabolites can contribute to antimicrobial resistance (AMR) while also destabilizing the critical bacterial populations needed for bio-filtration [13]. Second, conventional disinfection methods, though effective, are associated with the risks of manipulating toxic reagents and generating harmful disinfection by-products (DBPs), which endanger both the environment and public health [14].

* Corresponding author.
E-mail address: patricia.gmunoz@upm.es (P. García-Muñoz).

https://doi.org/10.1016/j.jece.2026.121589
Received 13 November 2025; Received in revised form 29 January 2026; Accepted 1 February 2026
Available online 2 February 2026

Advanced Oxidation Processes (AOPs) are recognized as a highly promising strategy for the remediation of persistent pollutants within water systems [15]. The foundation of these processes is the *in-situ* generation of powerful reactive oxygen species (ROS), which notably include hydroxyl radicals ($HO^{\bullet}$), sulfate radicals ($SO_4^{\bullet-}$), and singlet oxygen ($^1O_2$) [16,17]. These species leverage strong oxidative potential to efficiently decompose a wide array of organic, inorganic, and microbiological pollutants, establishing AOPs as a versatile water treatment solution [18–20]. Their efficacy is derived from the ability to degrade contaminants via multiple reaction pathways, such as hydrogen abstraction, hydroxyl addition, and other redox-driven transformations [21]. This allows for the breakdown of complex molecules into less harmful compounds, ideally leading to their full mineralization into water and carbon dioxide. In aquaculture, AOPs are specifically applied to reduce organic waste, microbial pathogens, and antibiotic residues [22–24].

Photoassisted AOPs are investigated extensively for their versatile application in aquaculture, specifically for the removal of microorganisms and antibiotics [25–27]. Their operational mechanism is based on the radiation-based generation of ROS, which results from the reactivity of molecular excited states. These states are formed when energetic radiation (spanning the UV-C to solar range) interacts with the water matrix. Oxidizing species are frequently added to these systems [22,28,29], as their interaction with radiation can create a synergistic effect. This synergy enhances the decontamination and disinfection power of the technique [30–34].

As a subset of photoassisted AOPs, photocatalysis involves harnessing light energy to activate a solid semiconducting material [35,36]. The process is initiated when the semiconductor absorbs photons possessing energy equal to or greater than its bandgap. This absorption causes photoexcitation, leading to the creation of electron-hole pairs, which migrate to the catalyst's surface, where they engage in a redox cascade to generate potent oxidizing species [37]. The method's versatility and sustainability are key advantages, as it functions without harsh chemicals or high temperatures while being capable of attacking a wide array of contaminants, including microbial pathogens ([38]; [39]. Although titanium dioxide (TiO_2) was the traditional material, focus has recently shifted to wide-bandgap semiconductors and heterojunctions to enhance disinfection efficiency. Studies on ZnO nanostructures [40], Ag-doped titanium dioxide [41], and g-C_3N_4 composites [42] have demonstrated the versatility of photocatalysis in inactivating resistant pathogens ins aquaculture and wastewater matrices. In this context, the use of gallium trioxide (Ga_2O_3), as a wide-bandgap photocatalyst, opens the door to promising disinfection applications. Ga_2O_3 is notable for its excellent photostability [43], strong oxidative power, and high responsivity to UV-C irradiation due to its suitable bandgap (~4.8 eV) [44,45]. It is important to note that this ultra-wide bandgap inherently limits photoactivation to the UV-C range ($\lambda < 258$ nm), rendering visible light ineffective for the pristine material but ensuring an exceptionally high redox potential for deep oxidative disinfection. These properties make Ga_2O_3 an excellent candidate for water treatment systems designed to inactivate waterborne pathogens. In aquaculture, where microbial contamination presents significant health and ecological concerns [46], Ga_2O_3-based photocatalysis is a promising remediation pathway. Its effectiveness under UV-C irradiation can be further enhanced by combination with oxidants like peracetic acid (PAA), which promotes synergistic ROS generation [47].

The integration of such recyclable photocatalysts aligns with circular aquaculture goals by reducing chemical consumption and environmental footprint [48]. This photocatalytic approach emerges as a strategic tool for safer, low-impact disinfection in RAS, precisely because it minimizes DBP production [49], a well-documented health concern [50]. Conventional disinfectants, such as sodium hypochlorite (NaClO), react with organic matter and halogens in the water. This reaction forms toxic and carcinogenic DBPs, including chlorite (ClO_2^-), chlorate (ClO_3^-), and bromate (BrO_3^-) [51–53].

The primary objective of this research is to evaluate the inactivation of *Enterococcus faecalis* within aquaculture matrices using a Ga_2O_3/UV-C photocatalytic system, which is intensified by the addition of PAA and potassium peroxymonosulfate (PMS). After initial material characterization, the first experimental phase will determine the optimal radiation dosage, catalyst loading, and oxidant concentration, as well as the synergistic effect of these three components. Once optimal operational conditions are established, a comprehensive process assessment will follow, beginning with an evaluation of pH influence. The catalyst's reusability across multiple cycles will be tested, and *E. faecalis* regrowth will be monitored (0–1–3–7 days). A scavenging study will be conducted to identify the dominant ROS involved in the degradation. The process will then be validated in a real aquaculture matrix. Finally, an initial toxicological evaluation will be performed through three complementary analyses: monitoring for DBPs, measuring water quality parameters (WQPs) after treatment, and assessing the phytotoxicity of the treated effluents.

2. Materials and methods

2.1. Matrices of study

Simulated aquaculture water (SAW) is the matrix employed for the experiments of *E. faecalis* inactivation, and its and its preparation follows the protocol established in our previous work [54]. The chemical composition was designed to mimic the typical nutrient and organic loads of intensive RAS effluents as described by Van Rijn, utilizing ammonium chloride and yeast extract to simulate the inorganic nitrogen (TAN) and biodegradable organic carbon fractions, respectively [24]. SAW is composed of yeast extract (Sigma; 193.35 mg/L), ammonium chloride (NH_4Cl, Labkem; 26.28 mg/L), potassium dihydrogen phosphate (KH_2PO_4, Scharlau; 1.96 mg/L), sodium hydrogen carbonate, ($NaHCO_3$, Sigma; 0.31 mg/L), iron citrate, $FeC_6H_6O_7$ (Acros Organics; 0.31 mg/L), magnesium chloride ($MgCl_2$, Labkem; 50.0 mg/L), calcium chloride ($CaCl_2{\cdot}2\,H_2O$, Scharlau; 55.86 mg/L) and zinc sulfate ($ZnSO_4$, Labkem; 0.25 mg/L). The simulated matrix is also spiked with a strain of *Enterococcus faecalis* (ATCC 29212, Scharlab), prepared as detailed in Section 2.3 below, to reach an approximate concentration of $2.5{\cdot}10^5$ CFU/mL.

The real aquaculture matrix (Fish Tank Water, FTW) was collected from a Recirculating Aquaculture System (RAS) located at the *Escuela Técnica Superior de Ingeniería de Montes, Forestal y del Medio Natural* (UPM, Madrid). The facility operates a closed-loop system stocking Brown trout (*Salmo trutta*) and Cyprinids. The water treatment loop (whose diagram is represented in Figure S5 of the Supplementary Materials) includes mechanical separation via a drum filter, biological filtration for nitrification, and sand filtration, resulting in a stabilized effluent with a Dissolved Organic Carbon (DOC) content typical of functional RAS units (approx. 2.25 mg/L). Characterization of both matrices is available in Table S1 of the Supplementary Materials.

2.2. Chemical reagents

Reagent-grade Ga_2O_3 (Sigma-Aldrich) was employed as the semiconducting photocatalyst in this study. Gallium oxide (Ga_2O_3) exists in several polymorphic forms, with β-Ga_2O_3 being the most thermodynamically stable at ambient conditions [55]. This monoclinic phase is characterized by a wide band gap of 4.8 eV, making it suitable for UV-driven photocatalytic applications [44,56]. The material was used as purchased, without further purification or modification. The operational range of the assayed photocatalytic dosages was 25–250 mgGa_2O_3/L.

For the chemical intensification of the photocatalytic processes, peracetic acid (PAA, $C_2H_4O_3$, 15 % v/v; PanReac) and potassium peroxymonosulfate (PMS, $KHSO_5$-0.5$KHSO_4$-0.5K_2SO_4, reagent grade, Oxone®; Sigma-Aldrich) were employed. Their concentrations were assessed in the 0.01–0.05 mM range.

After completing the optimization of the radiation, catalyst and oxidant dosage, a scavenging study is performed. The selection of the scavenging agents was strictly based on their known second-order reaction rate constants (k) with specific ROS. tert-butanol (t-BuOH) was selected as a selective hydroxyl radical scavenger due to its high affinity ($k_{HO^\bullet} \approx 6.0{\cdot}10^8 M^{-1}s^{-1}$) and negligible reaction with singlet oxygen [57]. Methanol (MeOH) was employed to scavenge both hydroxyl and sulfate radicals ($k_{SO_4^{\bullet-},MeOH} \approx 1.1{\cdot}10^7 M^{-1}s^{-1}$, $k_{HO^\bullet,MeOH} = 9.7{\cdot}10^8\ M^{-1}s^{-1}$). Finally, Furfuryl Alcohol (FFA) was chosen for its high specificity towards single oxygen ($k_1O_2 \approx 1.2{\cdot}10^8 M^{-1}s^{-1}$) [58]. The dosage of the scavenging agents is selected with respect to the catalyst concentration, in a 20:1 ratio, to ensure quantitative reactivity of the generated ROS with the scavengers.

Additionally, reagent-grade quality hydrochloric acid (HCl, Sigma) and sodium hydroxide (NaOH, PanReac) are employed, in aqueous solution, to adjust the pH of the matrix for the corresponding study. Potassium iodide (KI, Chem-Lab) and sodium hydrogen carbonate, ($NaHCO_3$, Sigma) were employed for the detection of the residual PAA and PMS in the system.

2.3. Characterization of Ga_2O_3

Textural properties were evaluated by nitrogen adsorption–desorption isotherms using a Micromeritics ASAP 2420 analyzer. Measurements were performed at 77.3 K with nitrogen as the adsorptive gas. Prior to analysis, the sample was automatically degassed at 300 °C for 16 h. BET surface area, pore volume, and pore size distribution were obtained through standard BET, BJH, and t-plot analyses.

Surface morphology and elemental composition were assessed by scanning electron microscopy (SEM) coupled with energy-dispersive X-ray spectroscopy (EDS). SEM images were acquired at different magnifications to evaluate particle size and morphology. EDS spectra were collected under an accelerating voltage of 15 kV and an acquisition time of 60 s, using a normalized quantification method. The analyses provided both morphological information and semi-quantitative determination of the elemental composition, enabling verification of sample purity and the presence of gallium in the purchased material.

Crystalline phases were analyzed by X-ray diffraction (XRD) using Cu Kα radiation (λ = 1.5406 Å). The diffractograms were acquired in continuous mode over a suitable 2θ range, using standard instrumental settings to ensure phase resolution. XRD was employed in the reusability study to corroborate the stability of the material after 4 cycles of operation.

The point of zero charge (pH_{PZC}) was determined using the Mass Titration method. A catalyst concentration of 1.0 g/L was suspended in ultrapure water and stirred for 24 h until a stable equilibrium pH was reached. This limiting pH value is representative of the pH_{PZC} for pure metal oxides, following established protocols in literature [59,60].

2.4. Experimental procedure

100 mL of the *E. faecalis*-spiked matrix are treated in a batch UV-C photoreactor, which consists of a 250 mL Pyrex beaker under constant stirring and irradiated by a *PhotolabLED265–0.1er/cb* UV-C Lamp (Apria Systems, Ltd.) LED source emitting short-wave radiation with a peak at the 254 nm band, and an irradiance range of 0.5–2.5 W/m^2. 900 μL samples were extracted at the pertinent sampling times and immediately subjected to serial 10-fold dilutions (ranging from undiluted to 10^3 diluted) in sterile saline solution (0.9 % w/v NaCl) to ensure countable colony formation. The experimental setup is employed for all the optimization and process assessment studies in this work.

For the quantification of the residual PAA and PMS after the treatment, the oxidant concentration was monitored spectrophotometrically (METLER TOLEDO) using a procedure based on the iodometric method described by Liang et al. [61]. Briefly, sample aliquots were mixed with KI and sodium $NaHCO_3$, and the absorbance of the resulting yellow solution was measured at 351 nm.

For the Ga_2O_3 reutilization study, the semiconductor was decanted after treatment application, for 60 min. Due to the micrometric particle size and high density of the material, a 60-min decantation period was sufficient to ensure effective separation from the supernatant. Then, remaining reaction medium was extracted from the upper part of the reactor with a 50 mL syringe. Catalyst was washed with 3 cycles of 10 mL with ultrapure water and then dried at 50°C for 20 min. Then, it was resuspended in the corresponding matrix.

2.5. Microbiological analysis

The matrices were doped with a commercial *Enterococcus faecalis* strain (ATCC 29212, Scharlab). *E. faecalis* was selected as the model microorganism due to its role as a standard faecal indicator and its structural similarity to Gram-positive aquaculture pathogens (e.g., *Streptococcus* spp.). Its thick peptidoglycan cell wall provides higher resistance to oxidation compared to Gram-negative bacteria, ensuring a robust evaluation of the disinfection potential of the photocatalytic system.

For the preparation of the fresh bacterial stock culture, 20 mL of Luria-Bertani nutrient medium were inoculated with 200 μL of the strain and incubated at 37°C for 22 h. Then, the suspension was centrifugated at 4500 r.p.m. during 15 min, and the generated bacterial pellet reconstituted in 20 mL of sterile (0.9 % w/v) NaCl solution. 200 μL of this stock solution were spiked in the matrix, reaching the desired initial concentration.

For the quantification of *E. faecalis* in the disinfection experiments, the drop-plate method, with a detection limit of 100 CFU/mL is employed. A selective culture medium (Slanetz&Bartley; Condalab) is inoculated with serial 10-fold dilutions in sterile 0.9 % NaCl buffer solution; the spread plate method (Standard Method 9215 C) is employed to extend the detection limit to 10 CFU/mL. The counting of the appearing colonies is carried out after the incubation of the plates during 48 h at 37°C. The bacterial quantification is calculated with at least 10 replicates to ensure reproducibility and accuracy of the experiments.

For the performance of the bacterial regrowth study, the treated effluents from the optimized treatments are collected after their application and stored in the dark, at 20°C. The quantification of *E. faecalis* is performed analogously, with samples taken after 1, 3 and 7 days after treatment, in triplicate.

2.6. Disinfection by-products (DBPs) and water quality parameters (WQPs) determination

Ion Chromatography (IC) measurements are performed at the starting point and after culmination of the optimized inactivation experiments to assess the generation or abatement of anionic compounds in the aqueous matrix. For the IC measurements, an Eco IC Ion Chromatograph, with $Na_2CO_3/NaHCO_3$ 8.0/0.25 mM at a 0.7 mL/min flow as the mobile phase, is employed. The detection of the ionic analytes is carried out via conductometric measurements. The analysis targeted two groups of anions: (i) General Water Quality Parameters, featuring chloride (Cl^-), nitrite (NO_2^-), nitrate (NO_3^-), phosphate (PO_4^{3-}), sulfate (SO_4^{2-}), and acetate (CH_3COO^-); and (ii) Inorganic Disinfection By-Products, specifically chlorite (ClO_2^-), chlorate (ClO_3^-), and bromate (BrO_3^-).

For the determination of Total Organic Carbon (TOC) a Teledyne Tekmar TOC Torch equipped with combustion catalytic oxidation (700°C) + non-dispersive infrared detection (NDIR) is employed.

2.7. Phytotoxicity study

To assess the toxicity of the generated effluents, a phytotoxicity study based on seed germination is carried out. This study is based on the differences on the germination of different vegetal species when exposed

to the aqueous medium prior and after the photocatalytic treatments. *Raphanus sativus* (radish) and *Solanum lycopersicum* (tomato) were the selected vegetal species. For carrying out the experiment, 15 seeds of each species are placed on a Petri dish with a previously placed filtering paper, and 10 mL of the target sample are afterwards located. The seeds are incubated for 72 h at 25 ºC. After the incubation period, the germinated seeds were counted and the mean length of the stems of the species was measured. The germination index (GI) was calculated according to the Eq. 1:

$$GI(\%) = \frac{G_S * L_S}{G_C * L_C} * 100 \quad (1)$$

Where G_S and G_C are the number of seeds which have germinated after application of the sample effluent and the control, and L_S and L_C are the length (in millimetres) of the stems of such germinated plants.

2.8. Energy efficiency assessment

To evaluate the cost-effectiveness of the intensification strategy, the Electrical Energy per Order (E_{EO}) was calculated. This figure-of-merit, defined by the IUPAC [62], represents the electrical energy (kWh) required to reduce the concentration of a pollutant by one order of magnitude in 1 m^3 of water. For a batch reactor, it is defined as it shows in Eq. 2:

$$E_{EO} = \frac{P \cdot t \cdot 1000}{V \cdot 60 \cdot \log \frac{C_0}{C_f}} \quad (2)$$

Where P is the nominal power of the UV-C source (0.004 kW), t is the irradiation time (min), V is the volume of operation, and $\log(C_0/C_f)$ the achieved log-reduction.

3. Results and discussion

3.1. Characterization of the Ga_2O_3 material

SEM micrographs are presented in Fig. 1. The morphology and elemental composition of the commercial Ga_2O_3 were examined by SEM coupled with EDS. SEM images at low magnification (×300) reveal agglomerates of irregularly shaped particles distributed throughout the surface, whereas higher magnification (×3000 and x10000) highlights faceted grains with sharp edges and sizes in the micrometre range. These morphologies suggest a high degree of crystallinity and a preferential crystal growth. The EDS spectrum acquired on representative particles confirms the exclusive presence of gallium, without detectable impurities (Figure S1 in the Supplementary materials), thereby validating the purity of the material of work.

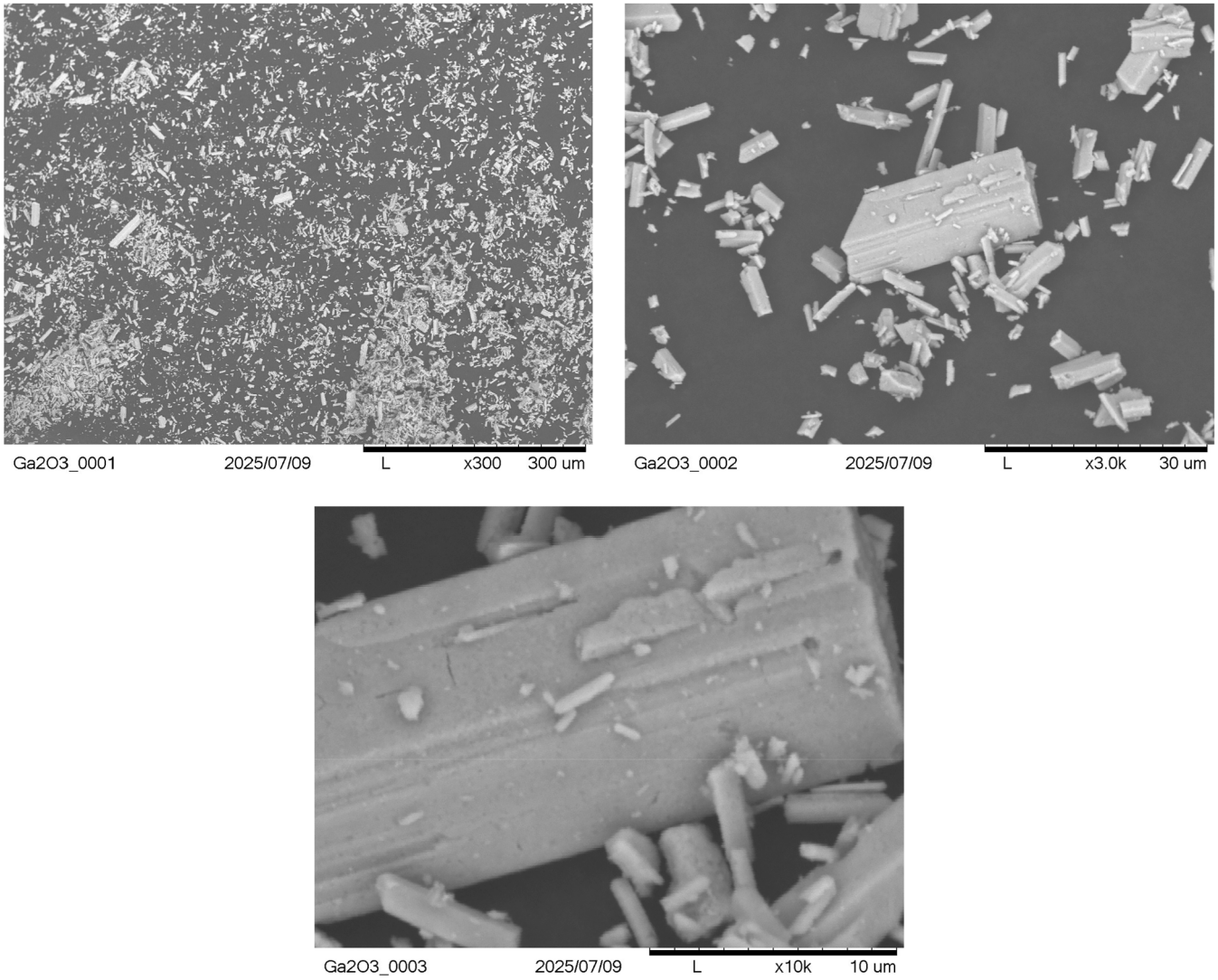

Fig. 1. Ga_2O_3 SEM micrographs, at 3.0k and 10k magnification.

The XRD diffractogram of the material is presented in Fig. 2, exhibiting intense and sharp peaks that match the monoclinic β-Ga_2O_3 phase (JCPDS 41–1103), with no additional reflections corresponding to secondary phases such as GaOOH or γ-Ga_2O_3. The pronounced peak intensity confirms the high crystallinity observed by SEM. Scherrer analysis of the main reflections (summarized in Table S2, Supplementary Materials) indicates crystallite sizes in the nanometric range, suggesting that the micrometer-sized grains observed in SEM are aggregates of smaller crystalline domains.

The nitrogen adsorption–desorption isotherms at 77 K are shown in Fig. 3. The sample exhibited a BET surface area of 5.37 m^2/g, with a pore volume of 0.029 cm^3 /g and an average pore size of ~22 nm. The t-plot analysis revealed a negligible microporous contribution, indicating that the surface is mainly composed of external facets. These values are within the typical range reported for crystalline β-Ga_2O_3 (<10 m^2/g) [63]. Although the surface area is relatively low compared to mesoporous photocatalysts, the photocatalytic performance of β-Ga_2O_3 is largely governed by its wide bandgap, high crystallinity, and ability to generate reactive oxygen species under UV irradiation, rather than solely by textural properties [64,65].

Overall, SEM–EDS, XRD and BET analyses confirm that the working material corresponds to pure, phase-stable β-Ga_2O_3, with micrometer-sized faceted grains composed of nanocrystalline domains and a low specific surface area. These structural and electronic features are expected to favour reproducible UV-C-assisted disinfection activity, where crystallinity and electronic properties dominate over porosity in determining the catalytic response.

3.2. Optimization of the UV-C and Ga_2O_3 dosage

As the first step in the optimization of the photocatalytic process, the UV-C radiation dosage is optimized. The initial application range is the 1.0 – 2.5 W/m^2. After light dosage assessment, the 1.0 W/m^2 intensity is selected for the rest of the experiment, since it is considered to allow the following of the bacterial inactivation kinetics while performing at a reasonable velocity in terms of quantitative disinfection during the maximum operational time, set in 15 min. The results are graphically represented in Fig. 4a.

Next, Ga_2O_3 dosage is optimized via the assessment of the bacterial inactivation with several concentrations (ranging 0.025–0.250 g/L) of the semiconductor under the stipulated 1.0 W/m^2 radiation intensity. The Ga_2O_3 dosage optimization results are represented in Fig. 4*b*. As it can be seen, the 0.025 and 0.100 gGa_2O_3/L concentrations improved the disinfection process with respect of the sole application of radiation, with the dosage of 0.250 gGa_2O_3/L showing a worse inactivation yield. This underperformance can be explained considering the aggregation of the catalyst above a threshold concentration, which diminishes its surface area and thus limits the photocatalytic activity. This tendency to aggregation has been confirmed by SEM measurements, Since the 0.025 g/L catalyst dosage is the one that exhibits a higher inactivation yield for the 1.0 W/m^2 radiation dosage, it will be selected as the optimum for the photocatalytic experiments.

A dark-phase inactivation study, with the only application of Ga_2O_3 in the dosage of work, was performed, showing that the material has no intrinsic antibacterial properties at any of the studied concentrations. This result is consistent with the relatively low surface area exhibited by the material. The results of the dark-phase experimentation are summarized in the Supplementary Materials, in Figure S2.

3.3. PAA and PMS intensification

The role of PAA and PMS as intensification agents in the photocatalytic process will be studied. The assessed dosages are preliminary selected according to a preliminary homogeneous-system study (in which only the effect of the oxidant and the radiation effects are evaluated) and are between the 0.01–0.05 mM range. The results of the preliminary homogeneous disinfection study are summarized in Figure S3, in the Supplementary Materials.

The results of the PAA intensification study are presented in Fig. 5:

The results show that the effect of the oxidant is only patent when the PAA dosage is at least of 0.02 mM. This oxidant concentration supposes a slightly quicker disinfection (from 5.5 to 5 min until below-LOD-

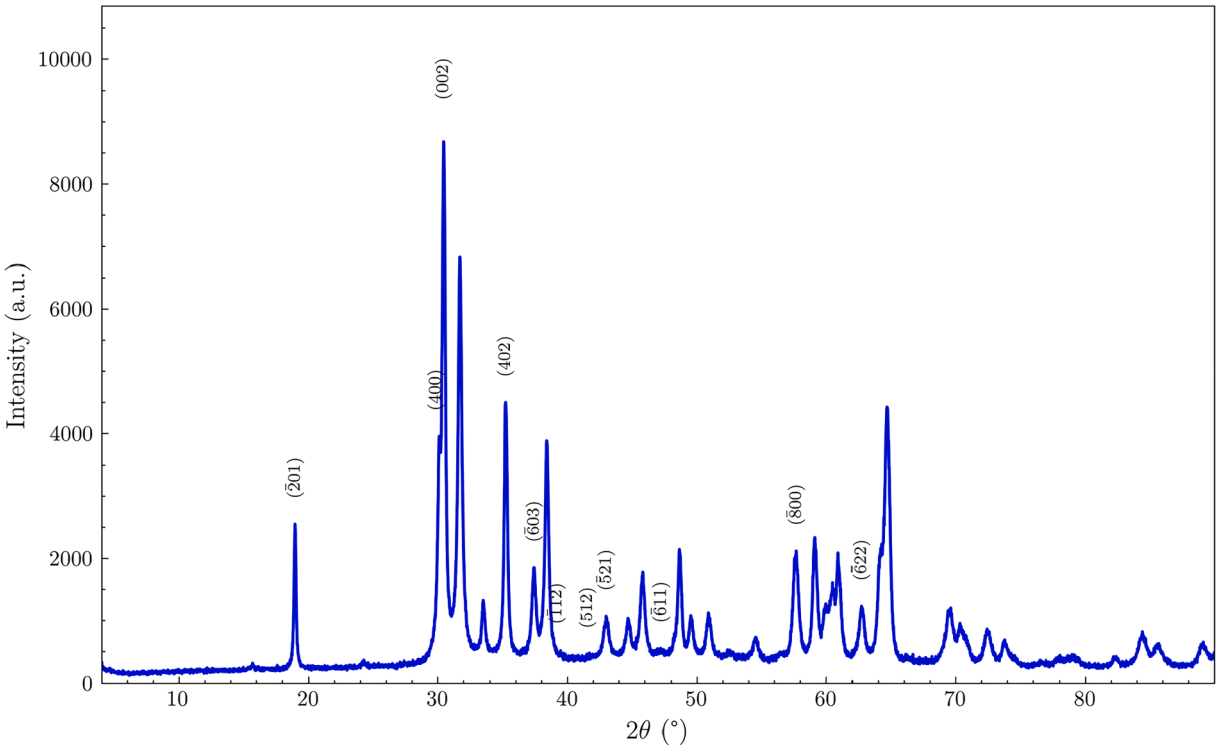

Fig. 2. XRD of the commercial Ga_2O_3.

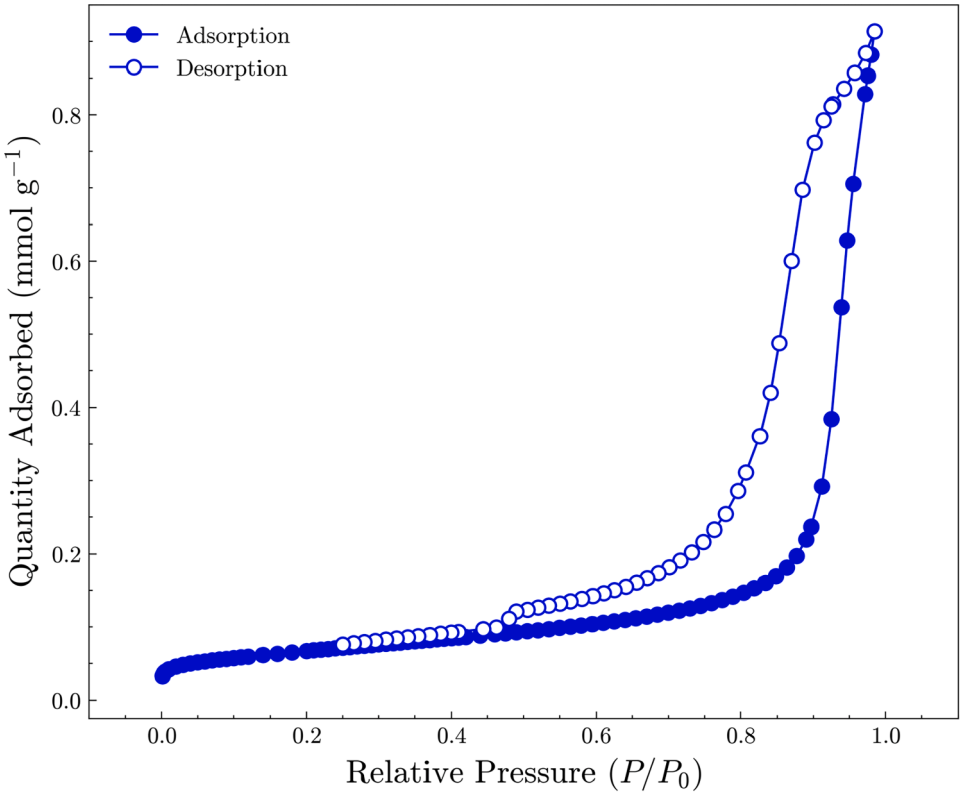

Fig. 3. Nitrogen adsorption–desorption isotherm of Ga_2O_3 at 77 K.

inactivation). However, the 0.05 mM concentration halves the time required for complete inactivation to 2.5 min, considerably accelerating the application of the process without compromising the following of the reaction. For this reason, this concentration is selected as the optimal for the Ga_2O_3/UV-C/PAA system and will be considered for all the following process assessment studies.

Beyond kinetic rates, the energy footprint was evaluated. The E_{EO} value decreased from 0.83 kWh/m^3 order in the Ga_2O_3/UV-C photocatalytic process to 0.38 kWh/m^3 order in the PAA-intensified system. This > 50 % reduction in energy demand confirms that the intensification strategy is economically advantageous for RAS applications.

PAA is known for its antimicrobial behaviour and its use in the intensification of photocatalytic processes. Drosou et al. explored the TiO_2/UV-A/PAA system, with oxidant dosages in the 0.5–2.0 mg/L range, for the disinfection of *E. coli* in sterile water, observing that the application of PAA at levels of 1.5 mg/L supposed a 5- log reduction in the bacterial population in 20 min of contact, while the increment in the PAA dosage to 2.0 mg/L shortened the inactivation time to 20 min [66].

The results of the PMS intensification experimentation are presented in Fig. 6.:

Although the combination of PMS with Ga_2O_3 was explored, the system exhibited an antagonistic behavior compared to UV-C/PMS alone. To elucidate the inhibitory effect observed in the Ga_2O_3/UV-C/PMS heterogeneous system compared to homogeneous photolysis (UV-C/PMS), oxidant consumption was quantified. PMS consumption data is summarized in Table 1 below:

Unexpectedly, PMS decomposition was significantly lower in the presence of the catalyst than in the UV-C-only control, for all the studied concentrations. This empirical evidence suggests that the antagonism is not caused by unproductive radical quenching: if the antagonism were driven by unproductive radical quenching on the catalyst surface (catalytic decomposition without disinfection), PMS consumption values would be comparable to or higher than those of the homogeneous system.

However, the reduced oxidant consumption correlates with the slower bacterial inactivation, confirming that competitive photon absorption (optical shielding) is the primary inhibitory mechanism [67]. The turbidity introduced by the suspended Ga_2O_3 particles attenuates the UV-C fluence available for PMS photolysis, hindering the homolytic cleavage of the peroxide bond and suppressing the generation of bulk sulfate and hydroxyl radicals [68].

The antagonism effect in the three agents renders the Ga_2O_3/UV-C/PMS unfit for this disinfection application, so the system will not be object of further study in this work. PAA is, in consequence, the only oxidant selected for the intensification of the photocatalytic process.

3.4. *Regrowth study*

To address the long-term inactivation of *E. faecalis* by the systems of interest, a regrowth study is conducted. The results of the experimental work are summarized in Fig. 7 below:

Different conclusions can be extracted from the experimental results. While bacterial regrowth appears in both systems since the first day of assessment, this microorganism reappearance is much faster in the case of the Ga_2O_3/UV-C system than in the case of the PAA-intensified process. The regrowth patterns suggest the transition of surviving bacteria into a Viable But Non-Culturable (VBNC) state. In the Ga_2O_3/UV-C system, bacterial mortality may be primarily attributed to the suffering of DNA damage, which can be enzymatically repaired, allowing for resuscitation and subsequent proliferation [69,70].

Conversely, the PAA-intensified system imposes severe oxidative stress on cell membranes and intracellular components, rendering repair mechanisms less effective. Furthermore, the residual presence of PAA and its main metabolites (acetic acid and acetate anion, which is determined *via* IC measurements) in the effluent creates a bacteriostatic environment [71]. This chemical pressure inhibits the metabolic recovery of VBNC cells, thereby preventing their reversion to a vegetative state and ensuring long-term biosecurity. For this reason, and after the

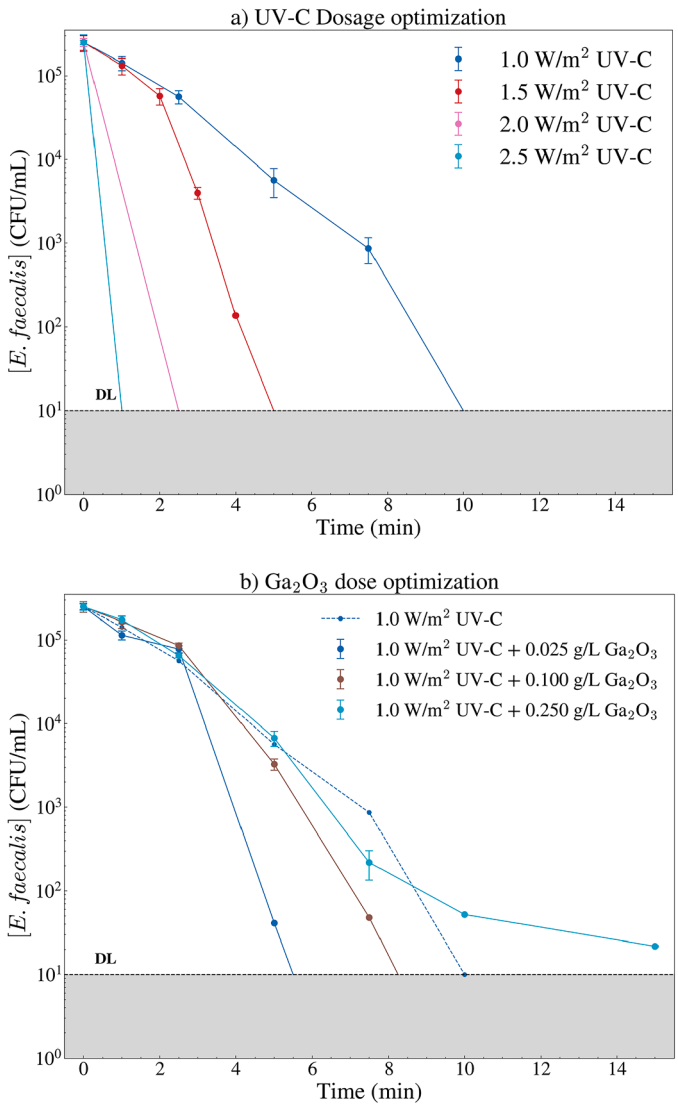

Fig. 4. UV-C (a) and Ga_2O_3 (b) optimization dosage for the *E. faecalis* inactivation process.

residual disinfection effect of PAA has been verified after treatment, an additional controlled PAA dosage could be applied to the treated effluent. According to Antonelli et al. [72], maintaining a residual concentration in the 0.5–1.0 mg/L range is effective for prolonging disinfection and preventing bacterial resuscitation. This polishing step would ensure long-term matrix biosecurity without introducing ecotoxicological risks [72].

Chong et al. addressed the regrowth of *E. coli* in photocatalytic systems using anatase titanate nanofibers as catalysts. They observed that the population of the bacteria recovered their initial levels after just 24 h of treatment for the photocatalytic system, while verified that the increasing presence of Fe^{2+} ions minimized bacterial regrowth, due to the residual generation of ROS species in the dark phase [73].

3.5. pH influence

The influence of the pH of the matrix, as the quintessential parameter in water systems, is addressed in this work. pH plays a critical role in photocatalysis, affecting the surface charge of the photocatalyst, as well as the generation and reactivity of ROS. A broad pH range of 4.5–10, selected considering the parameter range to which the microorganism is tolerant [74], will be assessed in this work. To understand these interactions, the pH_{PZC} of the Ga_2O_3 catalyst was determined to be 7.1 via the Mass Titration method.

The results of the experimentation are presented in Fig. 8.

The highest disinfection efficiency was achieved under neutral conditions (pH = 7.0), where 4.4-log reductions of *E. faecalis* were observed within less than 5.5 min. This optimal performance is attributed to several factors. Specifically, at pH 7.0, the catalyst operates near its pH_{PZC}, resulting in a near-neutral surface charge. This condition minimizes the electrostatic repulsion between the Ga_2O_3 particles and the negatively charged bacterial cell walls [75]. This lack of an electrostatic barrier facilitates a closer proximity between the microorganisms and the catalyst surface, where high concentrations of short-lived ROS are generated. This proximity, added to an enhanced ROS generation (based on the promotion of the oxidative activity of h^+ and subsequent formation of $HO^\bullet$ radicals) [76], is responsible to the high disinfection yield at pH neutrality. Disinfection performance is hindered at alkaline values of pH (pH = 10), which may be attributable to a suppression in the generation of $^1O_2$, a very pH sensitive process [77], to the scavenging of ROS by HO^- ions (which can quench the $HO^\bullet$ radicals through secondary reactions) [78], as well as the strong electrostatic repulsion of charge between the surface of the catalyst and the bacterial wall cell.

The results are in concordance with related photocatalytic literature, as optimal disinfection results are obtained when operating near neutral pH. The work carried out by Alikhani et al., where the ZnO/UV-C system was assessed for the disinfection of *E. coli*, showed optimal disinfection yields at pH values near neutrality, pointing to photochemical inactivation and surface interferences when operating at acidic or alkaline conditions [40]. In the study conducted by Sciscenko et al., where a catalyst based SiO_2/Fe_3O_4 coated with TiO_2 was employed in the UV-photocatalytic disinfection of *E. coli* and *C. perfringens*, authors report that the best operation conditions belonged in the circumneutral range of pH, ensuring no reagent addition and opening the door to catalyst recycling [79].

3.6. Ga_2O_3 reutilization

The capacity of maintaining the disinfection performance during several treatment cycles is a key parameter for the assessment of a photocatalyst. The inactivation curves for the catalyst reutilization study are presented in Fig. 9.

A notable reusability of the material is observed. During the four cycles of application, 4.40- log reduction of bacteria is observed in 7.5–10.5 min, which supposes an acceptable value of disinfection, below the stipulated limit time of 15 min.

The functional stability observed during the recycling tests was further corroborated by structural post-analysis using XRD. As shown in Fig. 10, the diffractograms of the fresh and used catalyst (after 4 cycles) are virtually indistinguishable. The characteristic diffraction peaks of the monoclinic β-polymorph were preserved without many remarkable shifts in the 2θ positions or appearance of new impurity phases, with only the intensity associated to the (111) peak experimenting a non-negligible decrease.

The preservation of the diffraction pattern confirms that the long-range order of the crystal lattice was maintained, ruling out phenomena such as amorphization, photocorrosion, or surface hydroxylation. This structural robustness aligns with the high thermodynamic stability reported for the β-Ga_2O_3 phase and explains the consistent kinetic performance observed throughout the reuse cycles [45].

The maintenance of antibacterial activity suggests that the β-Ga_2O_3 surface resists photocorrosion and irreversible fouling under the tested conditions. This aligns with the known properties of the β-polymorph, which is the most thermodynamically stable form of gallium oxide [55] and exhibits excellent photostability [43]. Unlike unstable photocatalysts that degrade upon UV exposure, the robustness of this material allows for effective recovery via simple washing, confirming its durability for RAS applications.

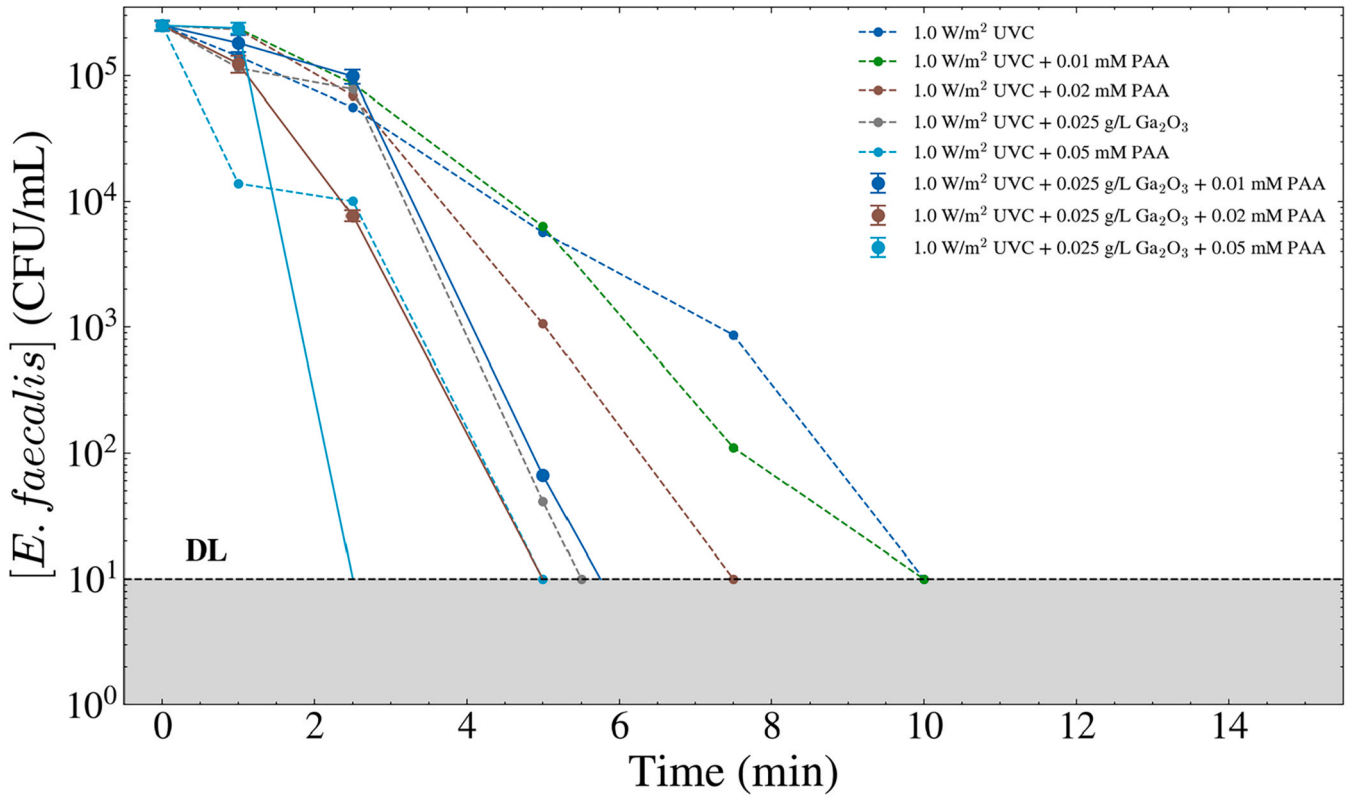

Fig. 5. PAA intensification of the Ga_2O_3/UV-C system. Influence of the oxidant dosage on *E. faecalis* inactivation.

Several studies have addressed the recyclability of the photocatalysts they employ. In the work by Fouad et al., a reusable coated $Ru/WO_3/ZrO_2$ material for the disinfection of gram-negative and gram-positive bacteria in presence of visible light. They observed that the recyclability of the material strongly depends on the matrix composition, as matrices with lower dissolved organic load enables a better reusability

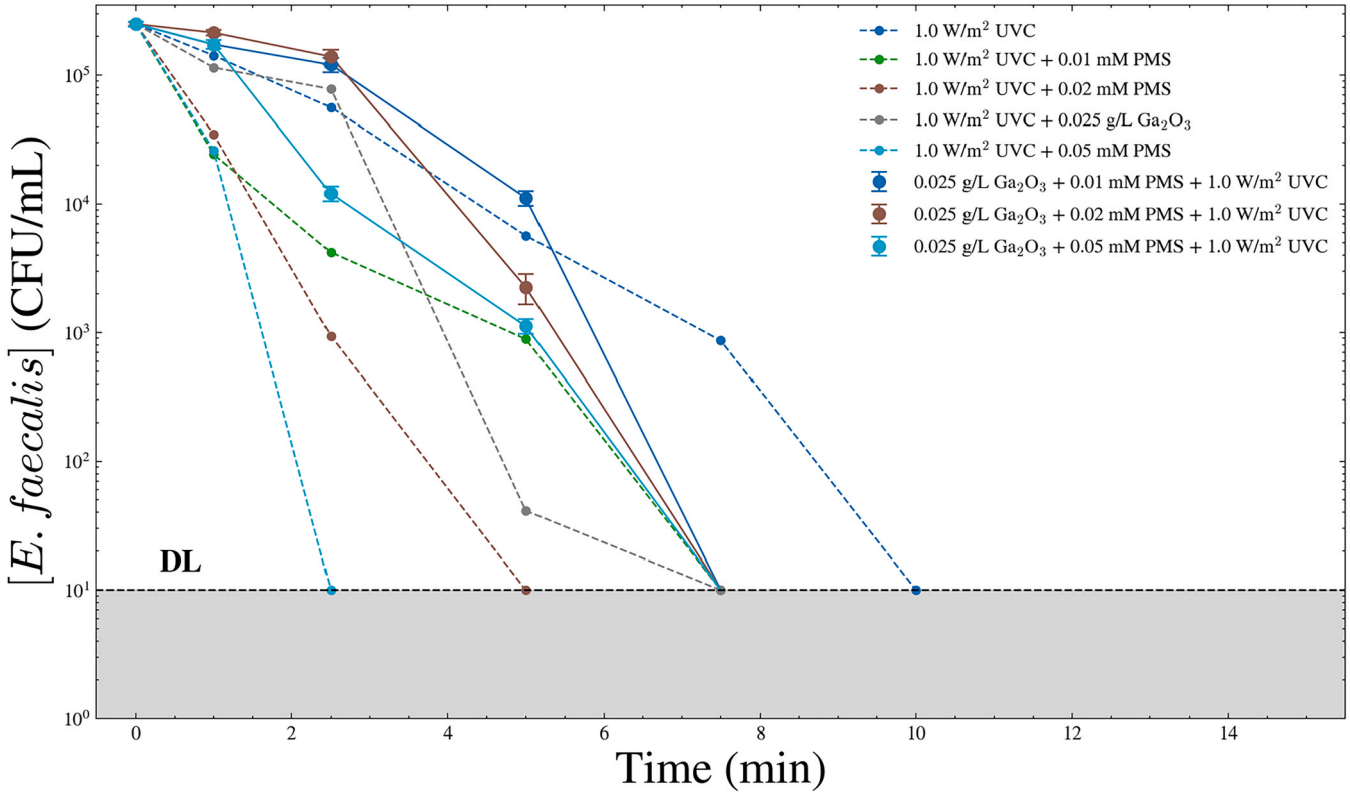

Fig. 6. PMS intensification of the Ga_2O_3/UV-C system. Influence of the oxidant dosage on *E. faecalis* inactivation.

Table 1
PMS Consumption for the Ga_2O_3/UV-C/PMS, UV-C/PMS and PMS systems.

	Normalized PMS consumption ([PMS] / [PMS]$_0$ ×100)		
Initial PMS dosage (mM)	**Ga_2O_3/UV-C/PMS**	**UV-C/PMS**	**PMS**
0.01	19.3	39.8	4.1
0.02	28.7	53.0	6.2
0.05	45.1	62.4	8.5

of the catalyst than their stronger counterparts [80]. Tsoukleris et al. addressed the inactivation of *E. coli* and other coliforms in municipal wastewater effluents employing chemically modified photocatalysts (N-TiO_2, N,S-TiO_2 and Ag@N-TiO_2) under visible light irradiation. They indirectly addressed the reusability of their materials by the comparison of the photodegradation yield of RhB dye solution after the first and fifth recycling run. While Ag@N-TiO_2 showed the better reusability performance, neither of the studied materials presented internal phase alterations, indicating the stability of their structure [81]. In the study by Cheng et al., addressing the reusability of FeClO in the FeClO/PAA system for the degradation of sulfamethoxazole. Their results point to a good reusability of the catalyst, since after solid washing and mild temperature drying (30°C), antibiotic degradations of at least 80 % were obtained, ensuring material integrity [82].

Inactivation yield stability, without major losing of photocatalytic activity during at least 4 cycles of reuse, combined to its swift performance, ensures the applicability of the catalyst for greater matrix volumes.

3.7. Real-water validation

Different inactivation yields for the Ga_2O_3/UV-C and Ga_2O_3/UV-C/PAA appear in the SAW and FTW matrices, as presented in Fig. 11.

Both systems of interest present faster inactivation yields in the FTW matrix than in the SAW, as it can be observed. Bacterial log 4.4 reduction in 2.5 and 1 min is achieved for the photocatalytic and intensified processes, respectively. This fast matrix disinfection may be explained by the difference in the organic load of the matrix (2.25 mg_{TOC} /L in FTW versus 56.68 mg_{TOC} /L in SAW). The presence of organic matter, which has reductive properties, competes for the oxidative power generated in the photocatalysis system, reducing its disinfection potential.

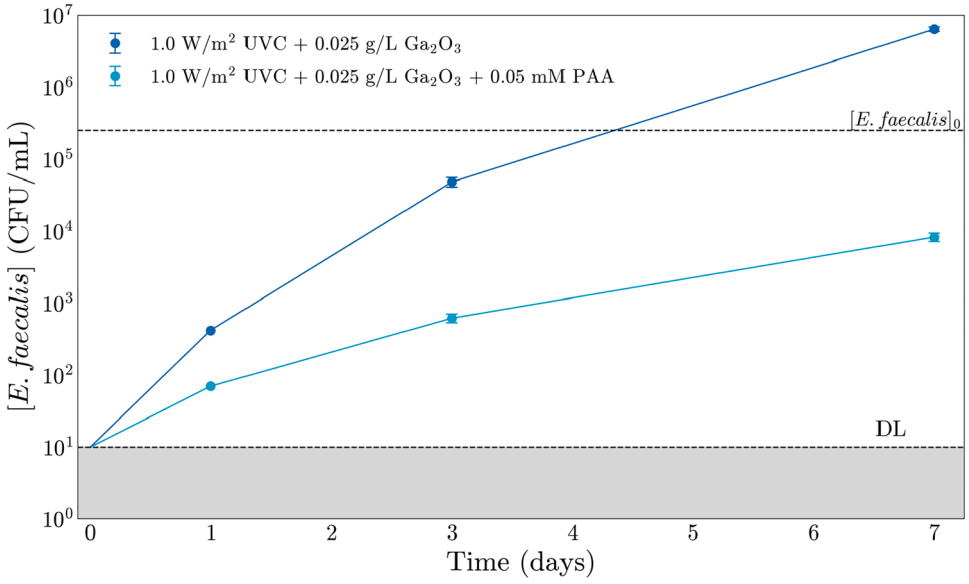

Fig. 7. Regrowth study. *E. faecalis* proliferation after the application of the optimized Ga_2O_3/UV-C and Ga_2O_3/UV-C/PAA processes.

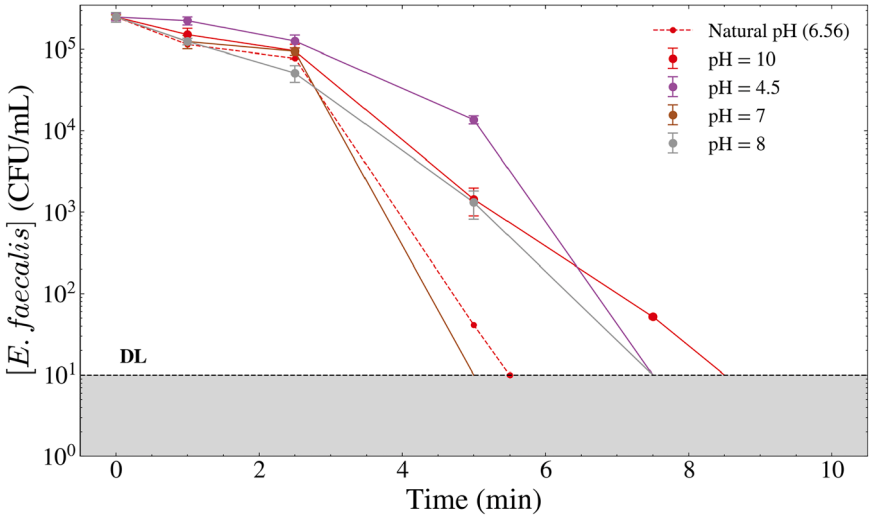

Fig. 8. pH influence study. *E. faecalis* inactivation under the optimized Ga_2O_3/UV-C process under several pH conditions.

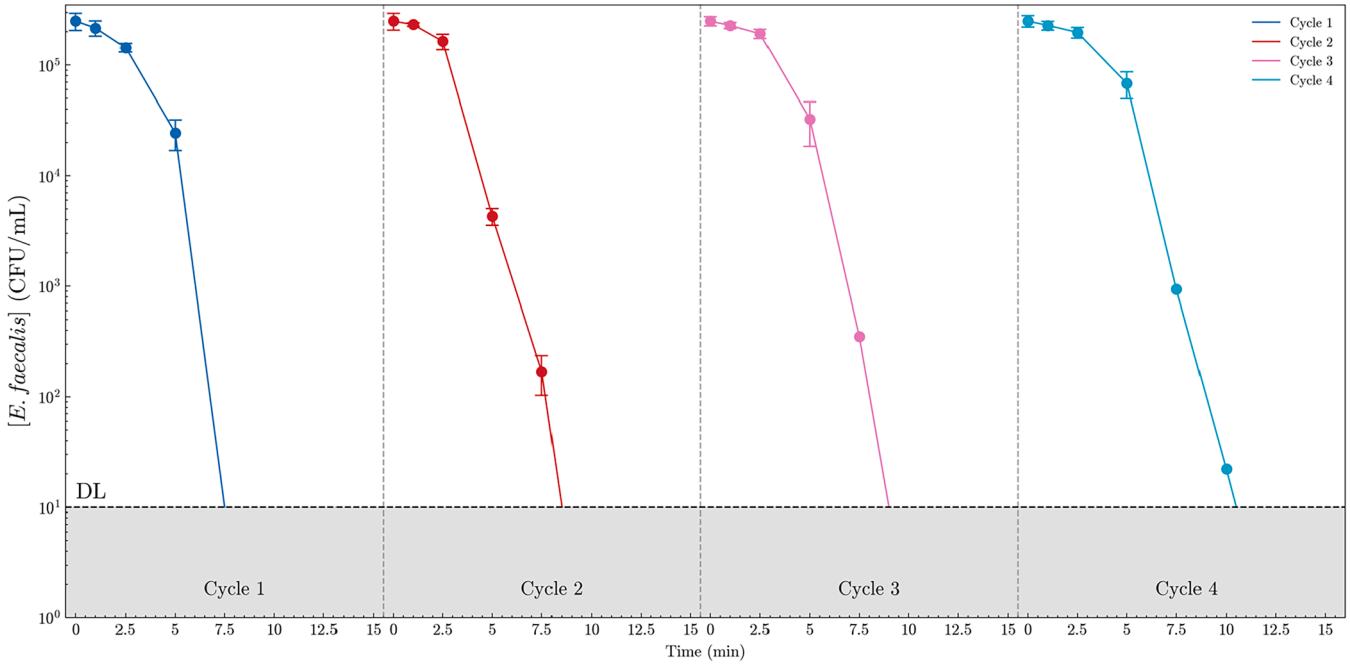

Fig. 9. *E. faecalis* inactivation yield in four consecutive cycles of application and reuse.

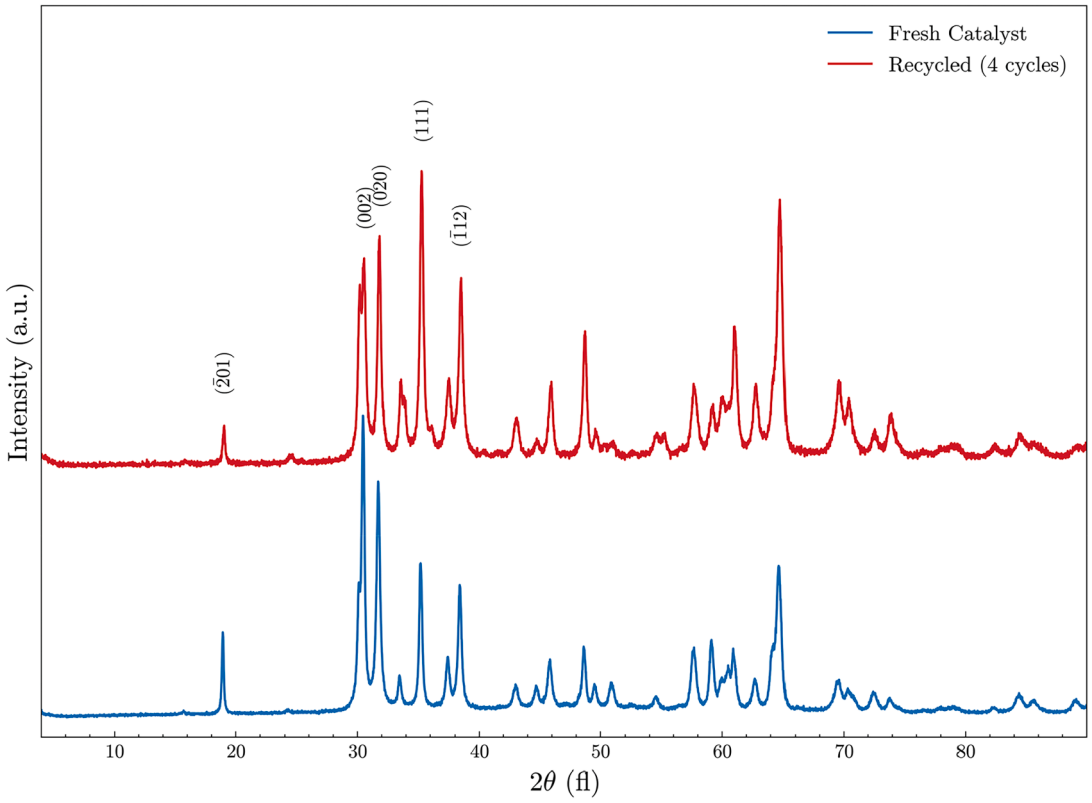

Fig. 10. Comparison of the XRD of the fresh and recycled Ga_2O_3 catalysts.

Higher matrix complexities are often associated with lower disinfection yields. In the study conducted by Xie et al., Graphitic Carbon Nitride semiconductor irradiated with visible light was applied for the inactivation of MS2 bacteriophage in several matrices with different organic loads. Their findings showed that matrices with 10 mg/L of dissolved organic carbon (DOC) reduced the yield of disinfection in 32–36 % of the process, attributing this drop in the performance to light absorption of the organic substance and the protective effect on the microbe [83]. Birben et al. performed solar photocatalytic disinfection on *E. coli* with P25-TiO_2 as a photocatalyst, analyzing the performance of the process in matrices with different complexities. They verified that the effect of organic matter in reducing the disinfection yield is greater

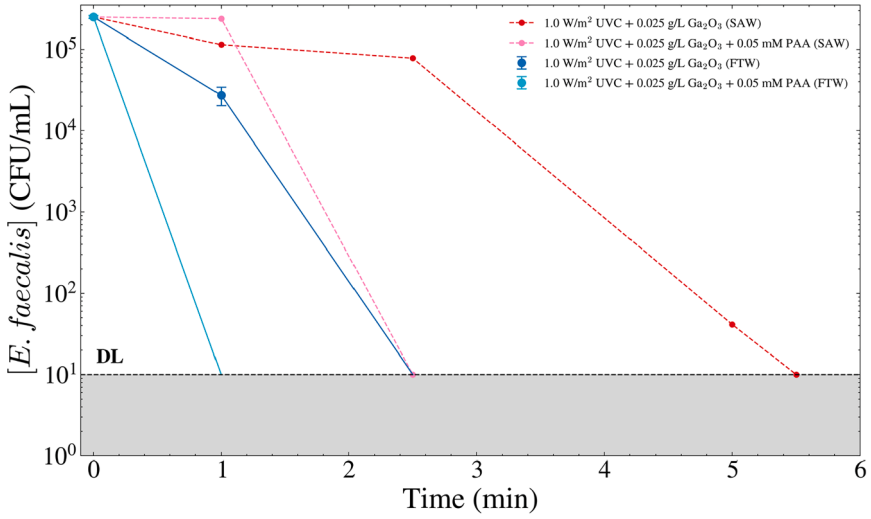

Fig. 11. Comparison of the *E. faecalis* inactivation yield of the studied processes in Simulated Aquaculture Water (SAW) and Fish Tank Water (FTW).

than the impact of saline composition, as the presence of organic matrices (in the form of humic acids), supposed a decrease in the inactivation rates in 4 orders of magnitude [84]. Ensuring matrix disinfection regardless its organic loading remains a challenge.

3.8. Toxicological considerations: phytotoxicity, DBPs and WQPs

The results of the phytotoxicity study are shown below, in Fig. 12.

As shown in Fig. 12, GI values for *R. sativus* and *S. lycopersicum* exposed to effluents from both the Ga_2O_3/UV-C and Ga_2O_3/UV-C/PAA treatments significantly exceeded the reference threshold of 100 %, indicating a stimulatory effect on seed germination and root growth. The observed phytostimulation for *R. sativus* and *S. lycopersicum* aligns with prior findings where AOPs not only mitigated microbial and chemical contaminants but also generated effluents with improved bioavailability of nutrients. The addition of PAA did not introduce phytotoxic effects; on the contrary, the intensified photocatalytic system resulted in germination indices comparable to, or slightly higher than, the non-intensified photocatalytic system. This suggests that the residual oxidants or their transformation products do not persist in phytotoxic concentrations, reinforcing the environmental safety of this AOP variant (specially at very low PAA concentrations) [85].

Importantly, the increase in GI in both systems indicates that the disinfection process did not lead to the accumulation of harmful by-products. This finding contrasts with some conventional disinfection techniques (e.g., chlorination), where the formation of phytotoxic halogenated by-products can impair germination [86]. These results support the viability of Ga_2O_3-based photocatalytic systems, especially when intensified with green oxidants like PAA, as environmentally sustainable technologies for aquaculture water treatment, capable of ensuring disinfection efficiency without compromising ecological thriving.

This potential of low-toxicity effluent generation is confirmed by the quantification of DBPs: no halogenated oxyanions (ClO_2^-, ClO_3^-, BrO_3^-) are detected above the operational limit of detection (0.1 mg/L) for any of the studied systems. While no specific legislation regulates the DBPs levels in aquaculture systems, the absence of these nefarious species is

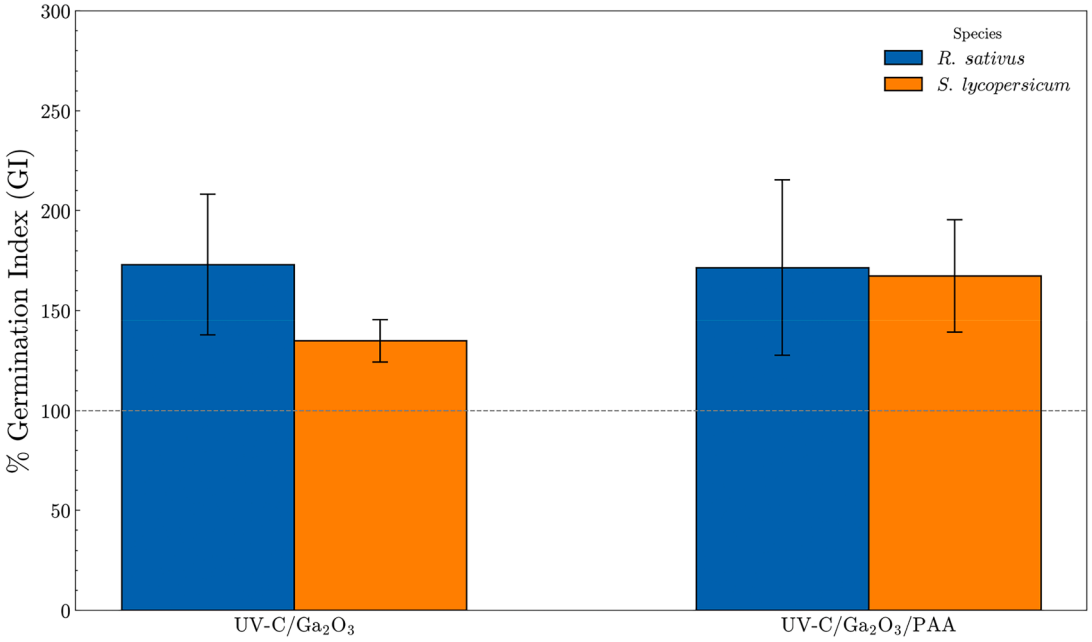

Fig. 12. Phytotoxicity of *Raphanus sativus* and *Solanum lycopersicum* for the Ga_2O_3/UV-C and Ga_2O_3/UV-C/PAA systems.

an optimistic result as the first step towards the scale-up of these advanced oxidation processes to industrial facilities.

The generation of DBPs in photocatalytic systems has gathered interest over the years; Richardson et. al assessed the performance of the UV/TiO_2 system in presence and absence and chlorination, observing that the generation of DBPs greatly decreased when the disinfection of ultrafiltered water was carried out by only application of photocatalytic processes, with 3-methyl-2,4-hexanedione being the only organic DBP that was detected [87]. The influence of the water matrix, addressed by Mayer et al., appears to not be the main factor in the production of DBPs in the TiO_2/UV system. Incomplete natural organic matter (NOM) oxidation drives the production of aromatic, humic-like DBPs, with authors reporting that only an intensive energy application can minimize the production of these residual substances [88]. The TiO_2/UV system is even a feasible approach to the treatment of disinfection by-products, as addressed by Zhang et al. In a non-conventional configuration of the TiO_2, featuring the encapsulation of the semiconducting material in sodium alginate hydrogel, the authors ensured significant (>96.4 %) removal of iodo-, bromo-, and chloroacetonitrile in deionized water after 60 min of treatment application [49].

The analysis of WQPs confirms that the variation of the chemical parameters in the matrix is minimal for the treatments of study. The main variations in the indicators are the generation of acetate in the Ga_2O_3/UV-C/PAA system, which is likely attributed to the chemical reduction of PAA [20], and the slight drop in the pH values for both treatments, which can be explained due to the generation of acidic species in the photocatalytic treatments [89] and the acidic behaviour of PAA. A minimal variation in the Cl^- concentration is likely attributed to the chloride appearing in the bacterial stock solution that is spiked in the matrix. Summarized variations in WQPs for the matrices of the study may be found in Figure S4, in the Supplementary Materials.

3.9. Scavenging study

The elucidation of the role of the different ROS taking part in the disinfection process is conducted via a scavenging study, whose results are presented in Fig. 13.

The disinfection profiles in presence of MeOH and tBuOH, which are respectively $HO^\bullet/SO_4^{\bullet-}$ and $HO^\bullet$ radicals scavengers [90,91], are similar for both studied processes (reaching complete disinfection at 7.5 min), which evidences the neglectable contribution of the sulfate radical in the systems. However, the increment in time to reach the detection limit is much higher for the PAA intensified system (from 2.5 to 7.5 min) than for Ga_2O_3/UV-C process (from 5.5 to 7.5 min). This notable increment in time points to a key role of the $HO^\bullet$ radical in the bacterial disinfection for the Ga_2O_3/UV-C/PAA system.

FFA acts as a selective scavenger for $^1O_2$ [92], a ROS having two different roles in the two processes of interest. The increment in the time to reach the detection limit of the PAA intensified process in presence of FFA is only of 2.5 min (from 2.5 to 5 min), but in the case of the Ga_2O_3/UV-C photocatalysis, complete disinfection is not only achieved in 15 min, but also it experiments a 2-log unit decrease. This behaviour highlights the key importance of $^1O_2$ in *E. faecalis* disinfection for the Ga_2O_3/UV-C system.

While no previous work has found on the mechanistic considerations of PAA-intensified UV-C disinfection by photocatalysis, the elucidation of the radical species involved in the UV/PAA disinfection of *E. coli* has been addressed by Sun et al. Their results showed that a 3.2-log decrease in inactivation appeared when an excess amount of t-BuOH was present in the disinfection set-up, evidencing the role of the $HO^\bullet$ radical in the disinfection process. These results are in concordance with the ones in the study conducted by Xu et al., where the UV/PAA process is applied for the inactivation of fungal spores in several matrices. Their findings point towards the importance of $HO^\bullet$ as the main radical participating in cell membrane damage [93].

$^1O_2$ apparition in photocatalytic systems has been attributed to the photoreduction of superoxide anion [94]. In the study by Cruz-Ortiz et al., the photocatalytic disinfection mechanism by Ti-graphene composites under UV radiation was modelled by the assessment of the *E. coli* disinfection. They concluded $^1O_2$, $HO^\bullet$ and H_2O_2 were the main responsible species in bacterial inactivation, with the non-detection of superoxide anion attributable to a fast rate of $^1O_2$ production [95].

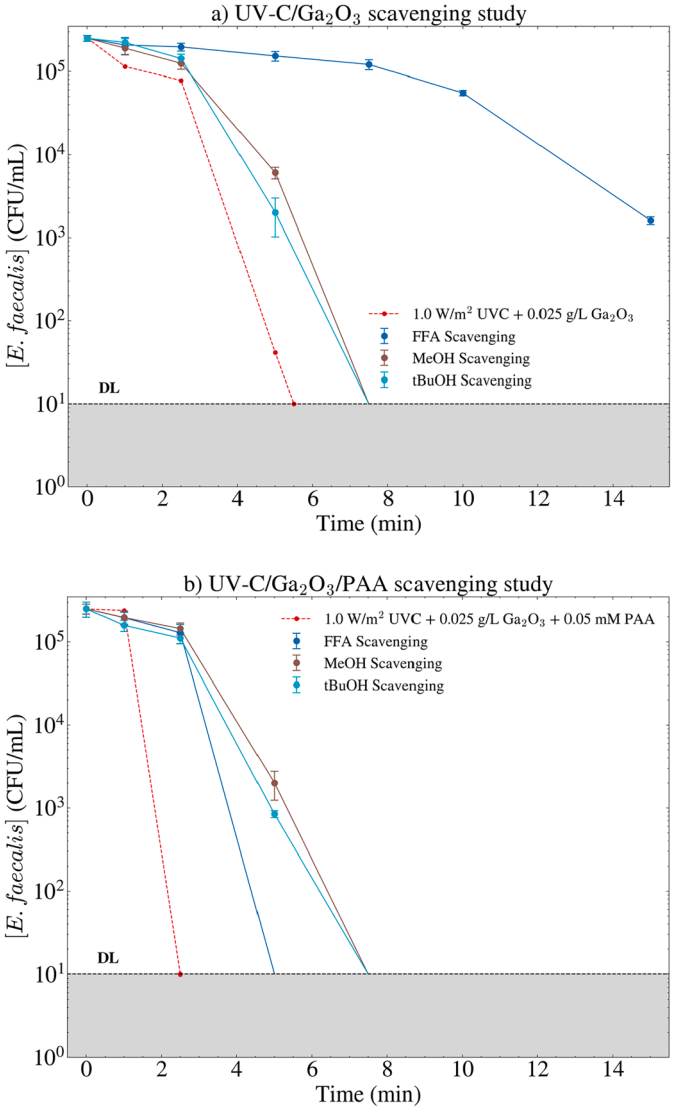

Fig. 13. Ga_2O_3/UV-C (a) and Ga_2O_3/UV-C/PAA (b) scavenging study for *E. faecalis* inactivation.

3.10. Proposal of an inactivation mechanism. Synergistic considerations

The disinfection performance observed for both the Ga_2O_3/UV-C and Ga_2O_3/UV-C/PAA systems point to distinct inactivation mechanisms, governed by the reactivity and dynamics of the generated ROS under each set of conditions. Based on experimental findings, particularly scavenging assays, a mechanistic proposal can be suggested to explain the observed pathways in bacterial inactivation.

The optimized Ga_2O_3/UV-C system achieved a complete inactivation of *E. faecalis* within 5.5 min, which was further accelerated to 2.5 min upon intensification with PAA. Scavenging tests were performed to estimate the contribution of different ROS. The addition of Furfuryl Alcohol (FFA) led to a significant inhibition of the process. While FFA is typically used as a probe for $^1O_2$, it is important to note that the deep valence band of β-Ga_2O_3 (E^0~4.0 V) thermodynamically favours the

generation of hydroxyl radicals and direct oxidation via valence band holes [96]. Therefore, the observed inhibition likely reflects a combined contribution of these oxidative species rather than the exclusive action of singlet oxygen.

Conversely, the Ga_2O_3/UV-C/PAA system showed an extended inactivation time in the presence of t-BuOH and MeOH. This is consistent with an intensification of the radical pathway, where the photolysis of PAA generates a higher flux of hydroxyl and peroxyl radicals, acting synergistically with the heterogeneous photocatalysis [97].

These observations are consistent with established ROS behaviour in photocatalytic and PAA-driven systems. Singlet oxygen generation in Ga_2O_3 photocatalysis can be attributed to energy transfer from photogenerated holes or by subsequent reduction of $O_2^{\bullet-}$ produced at the catalyst surface under UV-C excitation. Conversely, the presence of PAA favours the formation of $HO^{\bullet}$ through homolytic cleavage of the O-O bond in the oxidant initiated by UV-C absorption and its subsequent activation at the semiconductor surface.

A proposed mechanistic pathway for *E. faecalis* inactivation is described below for the Ga_2O_3/UV-C system, where the first step is the photocatalytic generation of electrons and holes after UV-C absorption of the semiconductor material, as presented in Eq. 3:

$$Ga_2O_3 \xrightarrow{UV-C} e^- + h^+ \quad (3)$$

Upon UV-C excitation, electron-hole pairs are generated. The high crystallinity of the β-Ga_2O_3 phase minimizes bulk defects, enhancing charge carrier mobility and reducing recombination [96]. The fate of these carriers determines the ROS profile, which may be generated by two different phenomena: the anodic and the cathodic pathway.

In the anodic pathway (h^+), the high potential associated to the valence band of the semiconductor material is significantly more positive than the redox potential for water oxidation ($E^0(H_2O/HO^{\bullet}) \sim +2.7$ V). Consequently, photogenerated holes (h^+) vigorously oxidize surface-adsorbed water molecules or hydroxide ions to generate $HO^{\bullet}$ radicals, which then attack the bacterial cell wall via hydrogen abstraction and hydroxylation:

$$h^+ + H_2O \rightarrow HO^{\bullet} + H^+ \quad (4)$$

In the cathodic pathway (*e*-), photogenerated electrons (*e*-) reduce dissolved oxygen to yield $O_2^{\bullet-}$, as represented in Eq. 5. While superoxide radical possesses intrinsic oxidative behaviour, scavenging insights indicate that its primary contribution in this system is its transformation into $^1O_2$, in a process that can occur via hole-induced oxidation or spontaneous disproportionation [98].

$$e^- + O_2 \rightarrow O_2^{\bullet-} \rightarrow {}^1O_2 \quad (5)$$

$^1O_2$, as an electronically excited form of molecular oxygen, may oxidize unsaturated lipids yielding lipid peroxidation [99], modify sulphur-containing amino acids (causing loss of enzymatic function) [100], or damage purine bases leading to oxidative DNA lesions, inducing mutagenesis [101].

$HO^{\bullet}$ has the theoretical capacity of attacking all classes of biomolecules due to its great standard redox potential of 1.8–2.7 V [76]. This oxidative power may lead to the oxidation of phospholipids (which produces structural destabilization and loss of osmoregulatory control [102], protein hydroxylation leading to secondary, tertiary and quaternary structure loss [103], and direct DNA strand breaks causing replication and transcription failure [104].

The Ga_2O_3/UV-C/PAA, in which the previously detailed reactivity can be observed, features the PAA photoactivation as its key inactivation feature, as detailed in Eq. 6:

$$CH_3COOOH \xrightarrow{UV-C} CH_3COO^{\bullet} + HO^{\bullet} \quad (6)$$

While electron abstraction by h^+ or other oxidative species generated in the photocatalytic process can occur, as shown in Eq. 7:

$$CH_3COOOH \xrightarrow{h^+} \text{radicals}(HO^{\bullet},\ CH_3COO^{\bullet}) \quad (7)$$

$HO^{\bullet}$, as previously detailed, acts rapidly and non-selectively on wall cells, internal structures, and DNA strands, fastening cell death.

However, the mechanism is not limited to homogeneous photolysis. A synergistic interaction occurs at the semiconductor interface, where PAA acts as an electron scavenger. The photogenerated electrons in the conduction band of β-Ga_2O_3 are captured by the PAA molecules. This charge transfer effectively suppresses the electron-hole recombination, prolonging the lifetime of the oxidative holes and further enhancing the generation ROS compared to the individual processes.

For determining the interaction between the different agents intervening in the process, a calculation of the synergy index (S) is carried out. This calculation considers the logarithmic disinfection of the process of studied, divided by the logarithmic disinfection of the different factors and their corresponding interactions. The value for S can be calculated according to Eqs. 8 and 9, for the Ga_2O_3/UV-C and Ga_2O_3/UV-C/PAA processes, respectively [105]:

$$S = \frac{\log\left(\frac{N}{N_0}\right)_{Ga_2O_3/UV-C}}{\log\left(\frac{N}{N_0}\right)_{Ga_2O_3} + \log\left(\frac{N}{N_0}\right)_{UV-C}} \quad (8)$$

$$S = \frac{\log\left(\frac{N}{N_0}\right)_{Ga_2O_3/UV-C/PAA}}{\log\left(\frac{N}{N_0}\right)_{Ga_2O_3/UV-C} + \log\left(\frac{N}{N_0}\right)_{UV-C/PAA} + \log\left(\frac{N}{N_0}\right)_{Ga_2O_3/PAA} - \log\left(\frac{N}{N_0}\right)_{UV-C} - \log\left(\frac{N}{N_0}\right)_{Ga_2O_3} - \log\left(\frac{N}{N_0}\right)_{PAA}} \quad (9)$$

The $\log\frac{N}{N_0}$ will be calculated at the time at which below-the-detection-level disinfection is achieved by the two systems, being it 7.5 min for the photocatalytic system and 2.5 min for the PAA-intensified photocatalytic system.

Values of S are presented below, in Table 2:

As shown in Table 2, both the Ga_2O_3/UV-C and Ga_2O_3/UV-C/PAA systems display remarkable synergistic effects, with synergy indices (S) of 1.715 and 3.945, respectively. These values confirm that the combined application of disinfection agents results in significantly enhanced bacterial inactivation compared to the additive performance of the individual components of the disinfection processes. This effect, while very notable for the Ga_2O_3/UV-C process, is particularly remarkable for

Table 2
Synergy indices (S) for the Ga_2O_3/UV-C and Ga_2O_3/UV-C/PAA systems.

System	Cutoff time (min)	Synergy index (S)
Ga_2O_3/UV-C	7.5	1.715
Ga_2O_3/UV-C/PAA	2.5	3.945

the Ga_2O_3/UV-C/PAA system, which achieves nearly a four-fold increase in log-reduction beyond the expected sum of the respective binary contributions.

The synergistic interaction between UV-C, Ga_2O_3, and PAA enhances the ROS yield (increasing the disinfection rates), which increases the likelihood of multi-site damage and prevents bacterial recovery, as shown in the regrowth experiments.

The origin of this synergy likely stems from multiple interacting factors. In the case of the Ga_2O_3/UV-C system, synergy can be attributed to the generation of ROS on the Ga_2O_3 surface under UV-C irradiation, a phenomenon which does not occur in the dark. Gallium oxide, a photocatalyst acting as a n-type semiconductor with a suitable band gap, generates electron-hole pairs under UV-C exposure, producing oxidative species such as hydroxyl radicals and singlet oxygen, which contribute to microbial cell wall disruption and DNA oxidation [106]. These ROS work in tandem with the photolytic effects of UV-C, explaining the observed synergistic enhancement over UV-C or Ga_2O_3 alone.

For the Ga_2O_3/UV-C/PAA system, the synergy is even more pronounced. This intensification arises from the combined oxidative stress imposed by both photogenerated ROS and the radicals derived from peracetic acid decomposition, such as acetylperoxyl ($CH_3COO^{\bullet}$) and $HO^{\bullet}$ radicals [97]. UV-C irradiation not only facilitates the direct decomposition of PAA but also enhances electron transfer on the Ga_2O_3 surface, accelerating radical generation and sustaining oxidative attack over time [107]. Acetate, after PAA hydrolysis, may also act as another reducing species, accepting electrons and favouring ROS generation via non-radical pathways [108]. These phenomena explain the near quadrupling of the observed inactivation performance at the established time limit.

This synergistic quantification based on log-reduction, as opposed to alternative calculation by evaluation of the kinetic constants, offers a robust and mechanistically meaningful framework to assess combined disinfection processes, especially when assessing systems following several models of microorganism abatement. Similar approaches have been reported in previous literature assessing UV/chlorine [109] and UV/PAA [110] systems, where synergy was calculated based on enhanced log-reductions beyond theoretical additivity.

The shift in dominant ROS between systems is reflected in the inactivation kinetics. The Ga_2O_3/UV-C system, driven primarily by $^1O_2$, showed a slower but sustained inactivation rate, while the Ga_2O_3/UV-C/PAA system exhibited a faster log-linear decay pattern, characteristic of $HO^{\bullet}$ dominated reactions ([111]; [112]). The latter species is known for its near-diffusion-limited reaction rate with biological macromolecules (10^9–10^{10} $M^{-1}s^{-1}$) [113], supporting the rapid microbial cell damage observed.

4. Conclusions

This study demonstrates the high potential of Ga_2O_3/UV-C-based photocatalysis as an efficient and sustainable disinfection strategy for RAS effluents. After material characterization and through a comprehensive optimization process, featuring the adjusting of the irradiation intensity, Ga_2O_3 dosage, and oxidant selection, the Ga_2O_3/UV-C/PAA system was identified as the most effective configuration for the inactivation of *E. faecalis*. Compared to UV-C irradiation alone, which required 10 min for complete inactivation, the intensified system reduced the treatment time to 2.5 min (a 4-fold kinetic enhancement). The incorporation of a low concentration of PAA significantly enhanced the disinfection kinetics, halving the required treatment time without compromising the followability of the bacterial inactivation process. Notably, PMS addition resulted in an antagonistic effect, emphasizing the necessity of careful system integration and the potential for non-productive radical consumption pathways which ultimately hinder the disinfection of the matrix.

Mechanistic insights derived from the scavenging experiments revealed that hydroxyl radicals and singlet oxygen play key roles in the microbial inactivation, with $^1O_2$ being particularly relevant in the sole Ga_2O_3/UV-C system, and $HO^{\bullet}$ dominating the disinfection in the Ga_2O_3/UV-C/PAA process. The photostability and recyclability of Ga_2O_3 were validated through multiple treatment cycles, confirming its viability for repeated use without significant loss of activity.

Long-term assessments highlighted the superior regrowth suppression provided by the PAA-intensified system, likely due to bacteriostatic residual oxidants. However, to fully mitigate the observed delayed bacterial recovery in real scenarios, two strategies are proposed: (i) the application of a minimal downstream residual PAA dose to ensure continuous biosecurity, or (ii) the design of recirculation loops with hydraulic retention times shorter than the bacterial resuscitation period (<1–3 days), ensuring retreatment before significant proliferation occurs. Importantly, real-matrix validation demonstrated robust performance of the optimized systems in authentic aquaculture effluents.

The combined assessment of phytotoxicity, DBPs generation and WQPs evolution verified the strong potential of the Ga_2O_3/UV-C and Ga_2O_3/UV-C/PAA processes in real systems, as a first step towards process scale-up.

From an economic perspective, the intensified Ga_2O_3/UV-C/PAA system offers a compelling trade-off for RAS applications. While the use of Ga_2O_3 and PAA introduces material costs, the 50 % reduction in required contact time (2.5 min vs. 5.5 min) implies a proportional decrease in reactor size (CAPEX) and electrical energy consumption (OPEX). Furthermore, the segregation of the treatment unit from the rearing tanks allows for the safe recirculation of the treated water, as the low PAA dosage (0.05 mM) degrades into acetate, a non-toxic, biodegradable by-product compatible with the system's biofilters.

Altogether, this work positions Ga_2O_3/UV-C photocatalysis, especially when intensified with peracetic acid, as a technically valid alternative to conventional chemical disinfectants. Its ability to combine swift microbial inactivation and catalyst reusability paves the way for future scale-up. While the material demonstrated excellent stability in high-organic simulated matrices, future pilot-scale investigations should assess long-term mechanical durability and potential biofouling under continuous flow conditions, ensuring its seamless integration into advanced water treatment frameworks for sustainable aquaculture.

CRediT authorship contribution statement

Jorge Rodríguez-Chueca: Visualization, Validation, Resources, Project administration, Methodology, Investigation, Funding acquisition. **Patricia García-Muñoz:** Visualization, Validation, Resources, Project administration, Methodology, Investigation, Funding acquisition. **Pablo Santiago-Espiñeira:** Investigation, Formal analysis, Data curation, Conceptualization.

Declaration of Competing Interest

The authors declare that they have no known competing financial interests or personal relationships that could have appeared to influence the work reported in this paper.

Acknowledgements

This work has received financial support from Spanish MCIN/AEI/10.13039/501100011033 and "ERDF A way of making Europe", through project PHOTORAS (PID2021–128165OA-I00). Pablo Santiago-Espiñeira acknowledges grant PRE2022–102194 funded by MICIU/AEI/10.13039/501100011033 and "FSE Investing in your future". The team wishes to express their gratitude to the personnel in the Aquaculture Facility of the *Escuela Técnica Superior de Ingeniería de Montes, Forestal y del Medio Natural, Universidad Politécnica de Madrid*, for providing the water matrices of work and for their technical advising.

Appendix A. Supporting information

Supplementary data associated with this article can be found in the online version at doi:10.1016/j.jece.2026.121589.

Data availability

Data will be made available on request.

References

[1] P.J.G. Henriksson, M. Troell, L.K. Banks, B. Belton, M.C.M. Beveridge, D. H. Klinger, N. Pelletier, M.J. Phillips, N. Tran, Interventions for improving the productivity and environmental performance of global aquaculture for future food security, One Earth 4 (2021) 1220–1232, https://doi.org/10.1016/J.ONEEAR.2021.08.009.

[2] L. López-Mas, A. Claret, M.J. Reinders, M. Banovic, A. Krystallis, L. Guerrero, Farmed or wild fish? Segmenting European consumers based on their beliefs, Aquaculture 532 (2021) 735992, https://doi.org/10.1016/J.AQUACULTURE.2020.735992.

[3] M. van Dijk, T. Morley, M.L. Rau, Y. Saghai, A meta-analysis of projected global food demand and population at risk of hunger for the period 2010–2050, 2, Nat. Food 2021 2 (7) (2021) 494–501, https://doi.org/10.1038/s43016-021-00322-9.

[4] N. Aich, S. Nama, A. Biswal, T. Paul, A REVIEW ON RECIRCULATING AQUACULTURE SYSTEMS: CHALLENGES AND OPPORTUNITIES FOR SUSTAINABLE AQUACULTURE, Inno. Farm 5 (2020) 17–24.

[5] A.B. Dauda, A. Ajadi, A.S. Tola-Fabunmi, A.O. Akinwole, Waste production in aquaculture: Sources, components and managements in different culture systems, Aquac. Fish. 4 (2019) 81–88, https://doi.org/10.1016/J.AAF.2018.10.002.

[6] M. Badiola, O.C. Basurko, R. Piedrahita, P. Hundley, D. Mendiola, Energy use in Recirculating Aquaculture Systems (RAS): A review, Aquac. Eng. 81 (2018) 57–70, https://doi.org/10.1016/J.AQUAENG.2018.03.003.

[7] Z.M. Gichana, D. Liti, H. Waidbacher, W. Zollitsch, S. Drexler, J. Waikibia, Waste management in recirculating aquaculture system through bacteria dissimilation and plant assimilation, Aquac. Int. 26 (2018) 1541–1572, https://doi.org/10.1007/S10499-018-0303-X.

[8] P.G. Preena, V.J. Rejish Kumar, I.S.B. Singh, Nitrification and denitrification in recirculating aquaculture systems: the processes and players, Rev. Aquac. 13 (2021) 2053–2075, https://doi.org/10.1111/RAQ.12558.

[9] R. Xiao, Y. Wei, D. An, D. Li, X. Ta, Y. Wu, Q. Ren, A review on the research status and development trend of equipment in water treatment processes of recirculating aquaculture systems, Rev. Aquac. 11 (2019) 863–895, https://doi.org/10.1111/RAQ.12270.

[10] P. Lindholm-Lehto, Water quality monitoring in recirculating aquaculture systems, Aquac. Fish. Fish. 3 (2023) 113–131, https://doi.org/10.1002/AFF2.102.

[11] C. Mutuku, Z. Gazdag, S. Melegh, Occurrence of antibiotics and bacterial resistance genes in wastewater: resistance mechanisms and antimicrobial resistance control approaches, World J. Microbiol. Biotechnol. 38 (2022) 152, https://doi.org/10.1007/S11274-022-03334-0.

[12] E.S. Okeke, K.I. Chukwudozie, R. Nyaruaba, R.E. Ita, A. Oladipo, O. Ejeromedoghene, E.O. Atakpa, C.V. Agu, C.O. Okoye, Antibiotic resistance in aquaculture and aquatic organisms: a review of current nanotechnology applications for sustainable management, Environ. Sci. Pollut. Res. Int 29 (2022) 69241, https://doi.org/10.1007/S11356-022-22319-Y.

[13] N. Hemamalini, S.A. Shanmugam, A. Kathirvelpandian, A. Deepak, V. Kaliyamurthi, E. Suresh, A critical review on the antimicrobial resistance, antibiotic residue and metagenomics-assisted antimicrobial resistance gene detection in freshwater aquaculture environment, Aquac. Res. 53 (2022) 344–366, https://doi.org/10.1111/ARE.15601.

[14] C. Wang, Z. Ying, M. Ma, M. Huo, W. Yang, Degradation of Micropollutants by UV–Chlorine Treatment in Reclaimed Water: pH Effects, Formation of Disinfectant Byproducts, and Toxicity Assay, 11, 2639, Water 2019 11 (2019) 2639, https://doi.org/10.3390/W11122639.

[15] M.A. Oturan, J.J. Aaron, Advanced oxidation processes in water/wastewater treatment: Principles and applications. A review, Crit. Rev. Environ. Sci. Technol. 44 (2014) 2577–2641, https://doi.org/10.1080/10643389.2013.829765.

[16] J. Wang, S. Wang, Reactive species in advanced oxidation processes: Formation, identification and reaction mechanism, Chem. Eng. J. 401 (2020) 126158, https://doi.org/10.1016/J.CEJ.2020.126158.

[17] Krystynik, P., 2022. Advanced Oxidation Processes (AOPs) – Utilization of Hydroxyl Radical and Singlet Oxygen. https://doi.org/10.5772/INTECHOPEN.98189.

[18] E.M. Cuerda-Correa, M.F. Alexandre-Franco, C. Fernández-González, Advanced oxidation processes for the removal of antibiotics from water. An overview, Water (Switz.) 12 (2020), https://doi.org/10.3390/W12010102.

[19] O.S. Keen, K.G. Linden, Degradation of antibiotic activity during UV/H2O2 advanced oxidation and photolysis in wastewater effluent, Environ. Sci. Technol. 47 (2013) 13020–13030, https://doi.org/10.1021/ES402472X.

[20] C. Shi, C. Li, Y. Wang, J. Guo, S. Barry, Y. Zhang, N. Marmier, Review of Advanced Oxidation Processes Based on Peracetic Acid for Organic Pollutants, 14, 2309, Water 2022 14 (2022) 2309, https://doi.org/10.3390/W14152309.

[21] M. Xu, J. Deng, A. Cai, C. Ye, X. Ma, Q. Li, S. Zhou, X. Li, Synergistic effects of UVC and oxidants (PS vs. Chlorine) on carbamazepine attenuation: Mechanism, pathways, DBPs yield and toxicity assessment, Chem. Eng. J. 413 (2021) 127533, https://doi.org/10.1016/J.CEJ.2020.127533.

[22] L. Rodriguez-Gonzalez, S.L. Pettit, W. Zhao, J.T. Michaels, J.N. Kuhn, N. A. Alcantar, S.J. Ergas, Oxidation of off flavor compounds in recirculating aquaculture systems using UV-TiO2 photocatalysis, Aquaculture 502 (2019) 32–39, https://doi.org/10.1016/j.aquaculture.2018.12.022.

[23] Y. Shen, C. Chen, P. Li, X. Huang, Y. Li, Application of a smart pilot electrochemical system for recycling aquaculture seawater, Aquac. Int. 32 (2024) 197–213, https://doi.org/10.1007/s10499-023-01150-3.

[24] J. Van Rijn, Waste treatment in recirculating aquaculture systems, Aquac. Eng. 53 (2013) 49–56, https://doi.org/10.1016/J.AQUAENG.2012.11.010.

[25] V. Zorzi, A. Bertini, A. Robertson, A. Berardinelli, L. Palmisano, F. Parrino, The application of advanced oxidation processes including photocatalysis-based ones for the off-flavours removal (GSM and MIB) in recirculating aquaculture systems, Mol. Catal. 551 (2023) 113616, https://doi.org/10.1016/J.MCAT.2023.113616.

[26] J. Moreno-Andrés, J.J. Rueda-Márquez, T. Homola, J. Vielma, M.Á. Moríñigo, A. Mikola, M. Sillanpää, A. Acevedo-Merino, E. Nebot, I. Levchuk, A comparison of photolytic, photochemical and photocatalytic processes for disinfection of recirculation aquaculture systems (RAS) streams, Water Res 181 (2020), https://doi.org/10.1016/J.WATRES.2020.115928.

[27] M. Uyğun, M.K. Fırat, O. Antepli, F.N. Bulat, M.A. Hekimoğlu, M.K. Bağcı, F. Güleç, C. Suzer, İ. Köse, Ş. Saka, B. Kılınç, The Water Disinfection with Different Type UV Lamp Systems on Bacterial Load in Small Scale Recirculating Aquaculture Systems. Turk, J. Fish. Aquat. Sci. 24 (2024) TRJFAS23785, https://doi.org/10.4194/TRJFAS23785.

[28] P. García-Muñoz, C. López-Maxías, S. Guerra-Rodríguez, J. Carbajo, J.A. Casas, J. Rodríguez-Chueca, Photocatalytic activation of peroxymonosulfate using ilmenite (FeTiO3) for Enterococcus faecalis inactivation, J. Environ. Chem. Eng. 10 (2022) 108231, https://doi.org/10.1016/J.JECE.2022.108231.

[29] R. Li, X. Wu, Z. Han, L. Xu, L. Gan, Y. Zhang, F. Lu, H. Lin, X. Yang, M. Yan, W. Chu, H. Gong, Removal of antibiotic-resistant bacteria and genes by Solar-activated Ferrate/ Peroxymonosulfate: Efficiency in aquaculture wastewater and mechanism, Chem. Eng. J. 474 (2023) 145547, https://doi.org/10.1016/j.cej.2023.145547.

[30] J.Y. Chin, A.L. Ahmad, S.C. Low, Antibiotics oxytetracycline removal by photocatalyst titanium dioxide and graphitic carbon nitride in aquaculture wastewater, J. Environ. Manag. 343 (2023), https://doi.org/10.1016/J.JENVMAN.2023.118231.

[31] D.R. Santana, M.R. Espino-Estévez, D.E. Santiago, J.A.O. Méndez, O. González-Díaz, J.M. Doña-Rodríguez, Treatment of aquaculture wastewater contaminated with metronidazole by advanced oxidation techniques, Environ. Nanotechnol. Monit. Manag 8 (2017) 11–24, https://doi.org/10.1016/J.ENMM.2017.04.001.

[32] P. Santiago-Espiñeira, P. García-Muñoz, P. Campayo-Navarro, J. Rodríguez-Chueca, Harnessing UV-C photoassisted AOPs: Amoxicillin degradation, disinfection by-products formation, and Enterococcus faecalis inactivation in aquaculture water, J. Environ. Manag. 388 (2025) 125983, https://doi.org/10.1016/J.JENVMAN.2025.125983.

[33] V. Silva, J.F.A. Fernandes, M.C. Tomás, C.P. Silva, V. Calisto, M. Otero, D.L. D. Lima, Enhanced solar driven photocatalytic removal of antibiotics from aquaculture effluents by TiO2/carbon quantum dot composites, Catal. Today 419 (2023) 114150, https://doi.org/10.1016/j.cattod.2023.114150.

[34] A. Singh, B.P. Nenavathu, K. Dasauni, T. Kumar Nailwal, ROS-Mediated Aquaculture Wastewater Remediation Using TeO2-Deposited ZnO Nanotubes, Water Air Soil Pollut. 233 (2022) 192, https://doi.org/10.1007/s11270-022-05668-9.

[35] O. Baaloudj, I. Assadi, N. Nasrallah, A. El Jery, L. Khezami, A.A. Assadi, Simultaneous removal of antibiotics and inactivation of antibiotic-resistant bacteria by photocatalysis: A review, J. Water Process Eng. 42 (2021) 102089, https://doi.org/10.1016/J.JWPE.2021.102089.

[36] S. Kumari, K. Sharma, S. Korpal, J. Dalal, A. Kumar, N. Supreet, S. Kumar, S. Duhan, A comprehensive study on photocatalysis: materials and applications, CrystEngComm 26 (2024) 4886–4915, https://doi.org/10.1039/D4CE00630E.

[37] B. Rani, A.K. Nayak, N.K. Sahu, Fundamentals principle of photocatalysis, Nanostruct. Mater. Visible Light Photocatal. (2022) 1–22, https://doi.org/10.1016/B978-0-12-823018-3.00009-9.

[38] D.A. Keane, K.G. McGuigan, P.F. Ibáñez, M.I. Polo-López, J.A. Byrne, P.S. M. Dunlop, K. O'Shea, D.D. Dionysiou, S.C. Pillai, Solar photocatalysis for water disinfection: materials and reactor design, Catal. Sci. Technol. 4 (2014) 1211–1226, https://doi.org/10.1039/C4CY00006D.

[39] Xinru Li, Y. Chen, Y. Tao, L. Shen, Z. Xu, Z. Bian, H. Li, Challenges of photocatalysis and their coping strategies, Chem. Catal. 2 (2022) 1315–1345, https://doi.org/10.1016/J.CHECAT.2022.04.007.

[40] M.Y. Alikhani, S.M. Lee, J.K. Yang, M. Shirzad-Siboni, H. Peeri-Dogaheh, M. S. Khorasani, M.A. Nooshak, M.R. Samarghandi, Photocatalytic removal of Escherichia coli from aquatic solutions using synthesized ZnO nanoparticles: a kinetic study, Water Sci. Technol. 67 (2013) 557–563, https://doi.org/10.2166/WST.2012.593.

[41] S. Chirumbolo, D. Gibellini, L. Berto, C. Cirrito, A. Vella, G. Bjørklund, A. Sbarbati, P. Bernardi, U. Tirelli, TiO2–Ag–NP adhesive photocatalytic films able to disinfect living indoor spaces with a straightforward approach, 13, Sci. Rep. 2023 13 (1) (2023) 4200, https://doi.org/10.1038/s41598-023-31464-4.

[42] X. Yang, L. Sheng, Y. Ye, J. Sun, S. Geng, D. Ning, Y. Zhang, X. Sun, Insights into the disinfection enhancement of homojunction g-C3N4 photocatalyst from charge

transfer regulation and cell-surface attachment, Chem. Eng. J. 474 (2023) 145771, https://doi.org/10.1016/J.CEJ.2023.145771.
[43] J.H. Lee, T.A. Doan, Y.J. Park, H.T.M. Hoa, P.H. Phuong, D.T. Le, N.H. Hung, Q. T. Tran, H.S. Lee, J.H. Ryu, J.Y. Yoo, T.V. Cuong, Synthesis and Photocatalytic Activity of β-Ga2O3 Nanostructures for Decomposition of Formaldehyde under Deep Ultraviolet Irradiation, 10, 1105, Catalysts 2020 10 (2020) 1105, https://doi.org/10.3390/CATAL10101105.
[44] M. Jędrzejczyk, K. Zbudniewek, J. Rynkowski, V. Keller, J. Grams, A.M. Ruppert, N. Keller, Wide band gap Ga2O3 as efficient UV-C photocatalyst for gas-phase degradation applications, Environ. Sci. Pollut. Res. 24 (2017) 26792–26805, https://doi.org/10.1007/S11356-017-0253-2.
[45] Teherani, F.H., Khodaparast, G.A., Xu, Y.V., Wu, J., Dravid, V.P., Pavlidis, D., Razeghi, M., McClintock, R., Rogers, D.J., Park, J.-H., Magill, B.A., 2018. A review of the growth, doping, and applications of Beta-Ga2O3 thin films 25. https://doi.org/10.1117/12.2302471.
[46] C. Regmi, B. Joshi, S.K. Ray, G. Gyawali, R.P. Pandey, Understanding Mechanism of Photocatalytic Microbial Decontamination of Environmental Wastewater, Front. Chem. 6 (2018) 331121, https://doi.org/10.3389/FCHEM.2018.00033/BIBTEX.
[47] J. Rodríguez-Chueca, S. Giannakis, M. Marjanovic, M. Kohantorabi, M. R. Gholami, D. Grandjean, L.F. de Alencastro, C. Pulgarín, Solar-assisted bacterial disinfection and removal of contaminants of emerging concern by Fe2+-activated HSO5- vs. S2O82- in drinking water, Appl. Catal. B 248 (2019) 62–72, https://doi.org/10.1016/J.APCATB.2019.02.018.
[48] M. Masi, F. Adinolfi, Y. Vecchio, G.P. Agnusdei, B. Coluccia, Toward the Circular Economy in the Aquaculture Sector: Bibliometric, Network and Content Analyses, 16, 5405, Sustainability 2024 16 (2024) 5405, https://doi.org/10.3390/SU16135405.
[49] P. Zhang, U. Claudine, S. Raza, Q. Zhang, J. Ye, M. Liu, A. Hayat, T. Bashir, E. Ghasali, P. Sengodan, R. Zhang, Y. Orooji, Advanced photocatalytic treatment of aqueous disinfection by-products with sodium alginate hydrogel-encapsulated titanium dioxide and luminous powder: A synergistic mechanism, J. Environ. Chem. Eng. 13 (2025) 116317, https://doi.org/10.1016/J.JECE.2025.116317.
[50] H. Cui, X. Zhu, Y. Zhu, Y. Huang, B. Chen, Ecotoxicological effects of DBPs on freshwater phytoplankton communities in co-culture systems, J. Hazard. Mater. 421 (2022) 126679, https://doi.org/10.1016/J.JHAZMAT.2021.126679.
[51] H. Cui, B. Chen, Y. Jiang, Y. Tao, X. Zhu, Z. Cai, Toxicity of 17 Disinfection By-products to Different Trophic Levels of Aquatic Organisms: Ecological Risks and Mechanisms, Environ. Sci. Technol. 55 (2021) 10534–10541, https://doi.org/10.1021/ACS.EST.0C08796/ASSET/IMAGES/LARGE/ES0C08796_0006.JPEG.
[52] W. Gan, H. Huang, X. Yang, Z. Peng, G. Chen, Emerging investigators series: disinfection by-products in mixed chlorine dioxide and chlorine water treatment, Environ. Sci. (Camb. 2 (2016) 838–847, https://doi.org/10.1039/C6EW00061D.
[53] C. Li, D. Wang, X. Xu, Z. Wang, Formation of known and unknown disinfection by-products from natural organic matter fractions during chlorination, chloramination, and ozonation, Sci. Total Environ. 587588 (2017) 177–184, https://doi.org/10.1016/J.SCITOTENV.2017.02.108.
[54] P. Santiago-Espiñeira, P. García-Muñoz, P. Campayo-Navarro, J. Rodríguez-Chueca, Harnessing UV-C photoassisted AOPs: Amoxicillin degradation, disinfection by-products formation, and Enterococcus faecalis inactivation in aquaculture water, J. Environ. Manag. 388 (2025) 125983, https://doi.org/10.1016/J.JENVMAN.2025.125983.
[55] A. Petkov, D. Cherns, W.Y. Chen, J. Liu, J. Blevins, V. Gambin, M. Li, D. Liu, M. Kuball, Structural stability of β-Ga2O3under ion irradiation, Appl. Phys. Lett. 121 (2022) 171903, https://doi.org/10.1063/5.0120089/2834417.
[56] N.S. Jamwal, A. Kiani, Gallium Oxide Nanostructures: A Review of Synthesis, Properties and Applications, Nanomaterials 12 (2022), https://doi.org/10.3390/NANO12122061.
[57] G.V. Buxton, C.L. Greenstock, W.P. Helman, A.B. Ross, Critical Review of rate constants for reactions of hydrated electrons, hydrogen atoms and hydroxyl radicals (·OH/·O− in Aqueous Solution, J. Phys. Chem. Ref. Data 17 (1988) 513–886, https://doi.org/10.1063/1.555805.
[58] E. Appiani, R. Ossola, D.E. Latch, P.R. Erickson, K. McNeill, Aqueous singlet oxygen reaction kinetics of furfuryl alcohol: effect of temperature, pH, and salt content, Environ. Sci. Process. Impacts 19 (2017) 507–516, https://doi.org/10.1039/C6EM00646A.
[59] M. Kosmulski, The pH dependent surface charging and points of zero charge. X. Update, Adv. Colloid Interface Sci. 319 (2023), https://doi.org/10.1016/j.cis.2023.102973.
[60] J.S. Noh, J.A. Schwarz, Estimation of the point of zero charge of simple oxides by mass titration, J. Colloid Interface Sci. 130 (1989) 157–164, https://doi.org/10.1016/0021-9797(89)90086-6.
[61] C. Liang, C.F. Huang, N. Mohanty, R.M. Kurakalva, A rapid spectrophotometric determination of persulfate anion in ISCO, Chemosphere 73 (2008) 1540–1543, https://doi.org/10.1016/J.CHEMOSPHERE.2008.08.043.
[62] J.R. Bolton, K.G. Bircher, W. Tumas, C.A. Tolman, Figures-of-merit for the technical development and application of advanced oxidation technologies for both electric- and solar-driven systems, Pure Appl. Chem. 73 (2001) 627–637, https://doi.org/10.1351/PAC200173040627.
[63] A.S. Kilian, A. de Siervo, R. Landers, G.J.P. Abreu, M.S. Castro, T. Back, A. Pancotti, Unravelling the surface structure of β-Ga2O3 (100), RSC Adv. 13 (2023) 28042, https://doi.org/10.1039/D3RA04682F.
[64] K.A. Mengle, G. Shi, D. Bayerl, E. Kioupakis, First-Principles Calculations of the Near-Edge Optical Properties of \b{eta}-Ga2O3, Appl. Phys. Lett. 109 (2019), https://doi.org/10.1063/1.4968822.
[65] F. Ricci, F. Boschi, A. Baraldi, A. Filippetti, M. Higashiwaki, A. Kuramata, V. Fiorentini, R. Fornari, Theoretical and experimental investigation of optical absorption anisotropy in $β$-Ga2O3, J. Phys. Condens. Matter 28 (2015), https://doi.org/10.1088/0953-8984/28/22/224005.
[66] C. Drosou, A. Coz, N.P. Xekoukoulotakis, A. Moya, Y. Vergara, D. Mantzavinos, Peracetic acid-enhanced photocatalytic and sonophotocatalytic inactivation of E. coli in aqueous suspensions, J. Chem. Technol. Biotechnol. 85 (2010) 1049–1053, https://doi.org/10.1002/JCTB.2396.
[67] Z. Honarmandrad, X. Sun, Z. Wang, M. Naushad, G. Boczkaj, Activated persulfate and peroxymonosulfate based advanced oxidation processes (AOPs) for antibiotics degradation – A review, Water Resour. Ind. 29 (2023) 100194, https://doi.org/10.1016/J.WRI.2022.100194.
[68] F. Ghanbari, M. Moradi, Application of peroxymonosulfate and its activation methods for degradation of environmental organic pollutants: Review, Chem. Eng. J. 310 (2017) 41–62, https://doi.org/10.1016/J.CEJ.2016.10.064.
[69] M. Ben Said, O. Masahiro, A. Hassen, Detection of viable but non cultivable Escherichia coli after UV irradiation using a lytic Qβ phage, Ann. Microbiol 60 (2010) 121, https://doi.org/10.1007/S13213-010-0017-4.
[70] X. Hu, X. Wang, H. Ren, C. Li, B. Zhang, R. Shi, Y. Wang, S. Lu, Y. Li, Q. Lu, Z. Liu, P. Hu, Preliminary Study of the Characterization of the Viable but Noncultivable State of Yersinia enterocolitica Induced by Chloride and UV Irradiation, Microorganisms 12 (2024) 1778, https://doi.org/10.3390/MICROORGANISMS12091778/S1.
[71] S.L. Aalto, L. Madsen, L.F. Pedersen, Peracetic acid mode-of-action on aquaculture microbes evaluated by dual-staining flow cytometry, Aquaculture 578 (2024) 740129, https://doi.org/10.1016/j.aquaculture.2023.740129.
[72] M. Antonelli, A. Turolla, V. Mezzanotte, C. Nurizzo, Peracetic acid for secondary effluent disinfection: A comprehensive performance assessment, Water Sci. Technol. 68 (2013) 2638–2644, https://doi.org/10.2166/WST.2013.542.
[73] M. Nan Chong, B. Jin, H. Zhu, C. Saint, Bacterial inactivation kinetics, regrowth and synergistic competition in a photocatalytic disinfection system using anatase titanate nanofiber catalyst, J. Photochem. Photobiol. A Chem. 214 (2010) 1–9, https://doi.org/10.1016/j.jphotochem.2010.05.018.
[74] A. Efstratiou, T. Lamagni, C.E. Turner, Definition for Streptococcal Toxic Shock-Like Syndrome, 2-Volume Set, Infect. Dis. (2017) 1523–1536.e2, https://doi.org/10.1016/B978-0-7020-6285-8.00177-5.
[75] Y. Nosaka, A.Y. Nosaka, Generation and Detection of Reactive Oxygen Species in Photocatalysis, Chem. Rev. 117 (2017) 11302–11336, https://doi.org/10.1021/ACS.CHEMREV.7B00161/ASSET/IMAGES/MEDIUM/CR-2017-00161A_0001.GIF.
[76] F.A. Villamena, Chemistry of Reactive Species, React. Species Detect. Biol. (2017) 13–64, https://doi.org/10.1016/B978-0-12-420017-3.00005-0.
[77] A.V. Demyanenko, A.S. Bogomolov, N.V. Dozmorov, A.I. Svyatova, A. P. Pyryaeva, V.G. Goldort, S.A. Kochubei, A.V. Baklanov, Singlet Oxygen 1O2 in Photocatalysis on TiO2. Where Does It Come from? J. Phys. Chem. C. 123 (2019) 2175–2181, https://doi.org/10.1021/ACS.JPCC.8B09381/ASSET/IMAGES/MEDIUM/JP-2018-093812_0011.GIF.
[78] J. Wang, R. Zhuan, Degradation of antibiotics by advanced oxidation processes: An overview, Sci. Total Environ. 701 (2020) 135023, https://doi.org/10.1016/J.SCITOTENV.2019.135023.
[79] I. Sciscenko, S. Mestre, J. Climent, F. Valero, C. Escudero-Oñate, I. Oller, A. Arques, Magnetic Photocatalyst for Wastewater Tertiary Treatment at Pilot Plant Scale: Disinfection and Enrofloxacin Abatement, 13, 329, Water 2021 13 (2021) 329, https://doi.org/10.3390/W13030329.
[80] M. Fouad, M. Gar Alalm, H.K. El-Etriby, D.C. Boffito, S. Ookawara, T. Ohno, M. Fujii, Visible-light-driven photocatalytic disinfection of raw surface waters (300–5000 CFU/mL) using reusable coated Ru/WO3/ZrO2, J. Hazard. Mater. 402 (2021) 123514, https://doi.org/10.1016/J.JHAZMAT.2020.123514.
[81] D.S. Tsoukleris, M.A. Gatou, N. Lagopati, L. Sygellou, D.C. Christodouleas, P. Falaras, E.A. Pavlatou, Chemically Modified TiO2 Photocatalysts as an Alternative Disinfection Approach for Municipal Wastewater Treatment Plant Effluents, Water (Switz.) 15 (2023) 2052, https://doi.org/10.3390/W15112052/S1.
[82] X. Cheng, J. Lian, M. Jiang, L. An, Q. Fan, G. Zeng, P. Su, Y. Wu, T. Yang, J. Ma, Unraveling Role Ch3c(=O)Oo• Degrad. Emerg. Org. Contam. Via Boost. Act. Peracetic Acid. Iron Oxychloride Catal. (2023), https://doi.org/10.2139/SSRN.4548201.
[83] Y. Xie, Z. Zhang, Y. Zhao, Y. Han, C. Liu, Y. Sun, Effect of dissolved organic matter on the inactivation of bacteriophage MS2 by graphitic carbon nitride - based photocatalysis, J. Environ. Chem. Eng. 12 (2024) 112025, https://doi.org/10.1016/J.JECE.2024.112025.
[84] N.C. Birben, E. Lale, C.S. Uyguner-Demirel, M. Bekbolet, Elucidation of in-situ produced organic matrix effect on the solar photo/photocatalytic inactivation of E. coli, Catal. Today 380 (2021) 53–61, https://doi.org/10.1016/J.CATTOD.2021.04.025.
[85] J.K. Hong, S.J. Jang, Y.H. Lee, Y.S. Jo, J.G. Yun, H. Jo, C.J. Park, H.J. Kim, Reduced Bacterial Wilt in Tomato Plants by Bactericidal Peroxyacetic Acid Mixture Treatment, Plant Pathol. J. 34 (2018) 78, https://doi.org/10.5423/PPJ.NT.06.2017.0131.
[86] Álvaro, J.E., Moreno, S., Dianez, F., Santos, Mila, Alvaro, J.E., Santos, Milagrosa, Carrasco, G., Urrestarazu, M., 2015. Effects of peracetic acid disinfectant on the postharvest of some fresh vegetables. https://doi.org/10.1016/j.jfoodeng.2009.05.003.
[87] S.D. Richardson, A.D. Thruston, T.W. Collette, K.S. Patterson, B.W. Lykins, J. C. Ireland, Identification of Tio2/UV disinfection byproducts in drinking water,

Environ. Sci. Technol. 30 (1996) 3327–3334, https://doi.org/10.1021/ES960142M/ASSET/IMAGES/LARGE/ES960142MF00005.JPEG.
[88] B.K. Mayer, E. Daugherty, M. Abbaszadegan, Disinfection byproduct formation resulting from settled, filtered, and finished water treated by titanium dioxide photocatalysis, Chemosphere 117 (2014) 72–78, https://doi.org/10.1016/J.CHEMOSPHERE.2014.05.073.
[89] A.F. Alkaim, T.A. Kandiel, F.H. Hussein, R. Dillert, D.W. Bahnemann, Enhancing the photocatalytic activity of TiO2 by pH control: A case study for the degradation of EDTA, Catal. Sci. Technol. 3 (2013) 3216–3222, https://doi.org/10.1039/C3CY00494E.
[90] S.Q. Yang, Y.H. Cui, J.Y. Li, X.D. Lv, Z.Q. Liu, Determination methods for steady-state concentrations of HO• and SO4•− in electrochemical advanced oxidation processes, Chemosphere 261 (2020) 127658, https://doi.org/10.1016/J.CHEMOSPHERE.2020.127658.
[91] S.Y. Oh, J.H. Kim, Degradation of phenol by perborate in the presence of iron-bearing and carbonaceous materials, RSC Adv. 13 (2023) 32833–32841, https://doi.org/10.1039/D3RA06986A.
[92] E. Appiani, R. Ossola, D.E. Latch, P.R. Erickson, K. McNeill, Aqueous singlet oxygen reaction kinetics of furfuryl alcohol: effect of temperature, pH, and salt content, Environ. Sci. Process. Impacts 19 (2017) 507–516, https://doi.org/10.1039/C6EM00646A.
[93] X. Xu, J. Zuo, Q. Wan, R. Cao, H. Xu, K. Li, T. Huang, G. Wen, J. Ma, Effective inactivation of fungal spores by the combined UV/PAA: Synergistic effect and mechanisms, J. Hazard. Mater. 430 (2022), https://doi.org/10.1016/j.jhazmat.2022.128515.
[94] A.V. Demyanenko, A.S. Bogomolov, N.V. Dozmorov, A.I. Svyatova, A. P. Pyryaeva, V.G. Goldort, S.A. Kochubei, A.V. Baklanov, Singlet Oxygen 1O2 in Photocatalysis on TiO2. Where Does It Come from? J. Phys. Chem. C. 123 (2019) 2175–2181, https://doi.org/10.1021/ACS.JPCC.8B09381/ASSET/IMAGES/MEDIUM/JP-2018-093812_0011.GIF.
[95] B.R. Cruz-Ortiz, J.W.J. Hamilton, C. Pablos, L. Díaz-Jiménez, D.A. Cortés-Hernández, P.K. Sharma, M. Castro-Alférez, P. Fernández-Ibañez, P.S.M. Dunlop, J.A. Byrne, Mechanism of photocatalytic disinfection using titania-graphene composites under UV and visible irradiation, Chem. Eng. J. 316 (2017) 179–186, https://doi.org/10.1016/J.CEJ.2017.01.094.
[96] L.K. Ping, D.D. Berhanuddin, A.K. Mondal, P.S. Menon, M.A. Mohamed, Properties and perspectives of ultrawide bandgap Ga2O3 in optoelectronic applications, Chin. J. Phys. 73 (2021) 195–212, https://doi.org/10.1016/J.CJPH.2021.06.015.
[97] S. Correa-Sanchez, G.A. Peñuela, Peracetic acid-based advanced oxidation processes for the degradation of emerging pollutants: A critical review, J. Water Process Eng. 49 (2022) 102986, https://doi.org/10.1016/J.JWPE.2022.102986.
[98] W.H. Koppenol, Reactions involving singlet oxygen and the superoxide anion, 262, Nature 1976 262 (5567) (1976) 420–421, https://doi.org/10.1038/262420a0.
[99] A. Ayala, M.F. Muñoz, S. Argüelles, Lipid Peroxidation: Production, Metabolism, and Signaling Mechanisms of Malondialdehyde and 4-Hydroxy-2-Nonenal, Oxid. Med. Cell. Longev. 2014 (2014) 360438, https://doi.org/10.1155/2014/360438.
[100] A. Michaeli, J. Feitelson, REACTIVITY OF SINGLET OXYGEN TOWARD AMINO ACIDS AND PEPTIDES, Photochem. Photobio. 59 (1994) 284–289, https://doi.org/10.1111/J.1751-1097.1994.TB05035.X.
[101] E. Dumont, R. Grüber, E. Bignon, C. Morell, Y. Moreau, A. Monari, J.L. Ravanat, Probing the reactivity of singlet oxygen with purines, Nucleic Acids Res 44 (2016) 56–62, https://doi.org/10.1093/NAR/GKV1364.
[102] A. Rovetta, L. Carosella, F. Arrigoni, J. Vertemara, L. De Gioia, G. Zampella, L. Bertini, Oxidation of Phospholipids by OH Radical Coordinated to Copper Amyloid-β Peptide—A Density Functional Theory Modeling †, Inorg. (Basel) 11 (2023) 227, https://doi.org/10.3390/INORGANICS11060227/S1.
[103] K.J. Davies, S.W. Lin, R.E. Pacifici, Protein damage and degradation by oxygen radicals. IV. Degradation of denatured protein, J. Biol. Chem. 262 (1987) 9914–9920, https://doi.org/10.1016/S0021-9258(18)48021-0.
[104] B. Balasubramanian, W.K. Pogozelski, T.D. Tullius, DNA strand breaking by the hydroxyl radical is governed by the accessible surface areas of the hydrogen atoms of the DNA backbone, Proc. Natl. Acad. Sci. U. S. A. 95 (1998) 9738–9743, https://doi.org/10.1073/PNAS.95.17.9738.
[105] A. Hassani, P. Eghbali, F. Mahdipour, S. Wacławek, K.Y.A. Lin, F. Ghanbari, Insights into the synergistic role of photocatalytic activation of peroxymonosulfate by UVA-LED irradiation over CoFe2O4-rGO nanocomposite towards effective Bisphenol A degradation: Performance, mineralization, and activation mechanism, Chem. Eng. J. 453 (2023) 139556, https://doi.org/10.1016/J.CEJ.2022.139556.
[106] S. Zhang, Y. Wang, J. Lu, Z. Yu, H. Song, P.L. Bond, J. Guo, Chlorine disinfection facilitates natural transformation through ROS-mediated oxidative stress, ISME J. 15 (2021) 2969–2985, https://doi.org/10.1038/S41396-021-00980-4.
[107] X. Chang, H. Zhang, X. Liu, W. Li, S. Kang, D. Sun, Z. Xiong, Photocatalysis enhancement and Cl− boosting mechanisms of peracetic acid-based advanced oxidation processes for antibiotic removal by using HOF-Cu-g-C3N4, N. J. Chem. 48 (2023) 322–331, https://doi.org/10.1039/D3NJ04090A.
[108] H. Zhang, G. Xu, Y. Yu, Photocatalytic activation of peracetic acid by metal–free C2N3 for efficient water purification under visible light: High–efficiency bifurcated electron transport, Chem. Eng. J. 485 (2024) 150035, https://doi.org/10.1016/J.CEJ.2024.150035.
[109] Y. Gao, Z. Sun, Y. Guo, Z. Qiang, W. Ben, Virus inactivation by sequential ultraviolet-chlorine disinfection: Synergistic effect and mechanism, Chemosphere 314 (2023) 137632, https://doi.org/10.1016/J.CHEMOSPHERE.2022.137632.
[110] Y. Bai, Yuanhang Zhou, R. Chang, Yingying Zhou, X. Hu, J. Hu, C. Yang, J. Chen, Z. Zhang, J. Yao, Investigating synergism and mechanism during sequential inactivation of Staphylococcus aureus with ultrasound followed by UV/peracetic acid, J. Hazard. Mater. 462 (2024) 132609, https://doi.org/10.1016/J.JHAZMAT.2023.132609.
[111] M.N. Chong, B. Jin, H. Zhu, C. Saint, Bacterial inactivation kinetics, regrowth and synergistic competition in a photocatalytic disinfection system using anatase titanate nanofiber catalyst, J. Photochem. Photobiol. A Chem. 214 (2010) 1–9, https://doi.org/10.1016/J.JPHOTOCHEM.2010.05.018.
[112] Xiang Li, Y. Zhang, X. Du, J. Cai, L. Gan, Q. Zhang, J. Jiang, Z. Li, Y. Sun, D. Liu, M. Yi, F. Chang, H. Li, Y. Du, A Review of Sulfate Radical-Based and Singlet Oxygen-Based Advanced Oxidation Technologies: Recent Advances and Prospects, 12, 1092. Catalysts 2022 12 (2022) 1092, https://doi.org/10.3390/CATAL12101092.
[113] G.V. Buxton, C.L. Greenstock, W.P. Helman, A.B. Ross, Critical Review of rate constants for reactions of hydrated electrons, hydrogen atoms and hydroxyl radicals (·OH/·O− in Aqueous Solution, J. Phys. Chem. Ref. Data 17 (1988) 513–886, https://doi.org/10.1063/1.555805.